Graphical Abstract

Characterization of the critical lift-off of a single flat-plate microchip particle in straight rectangular microchannel flows

Raymond Yeung, Cynthia Sainz, Jason Mandala, Philip Brisk, William H. Grover, Victor G. J. Rodgers

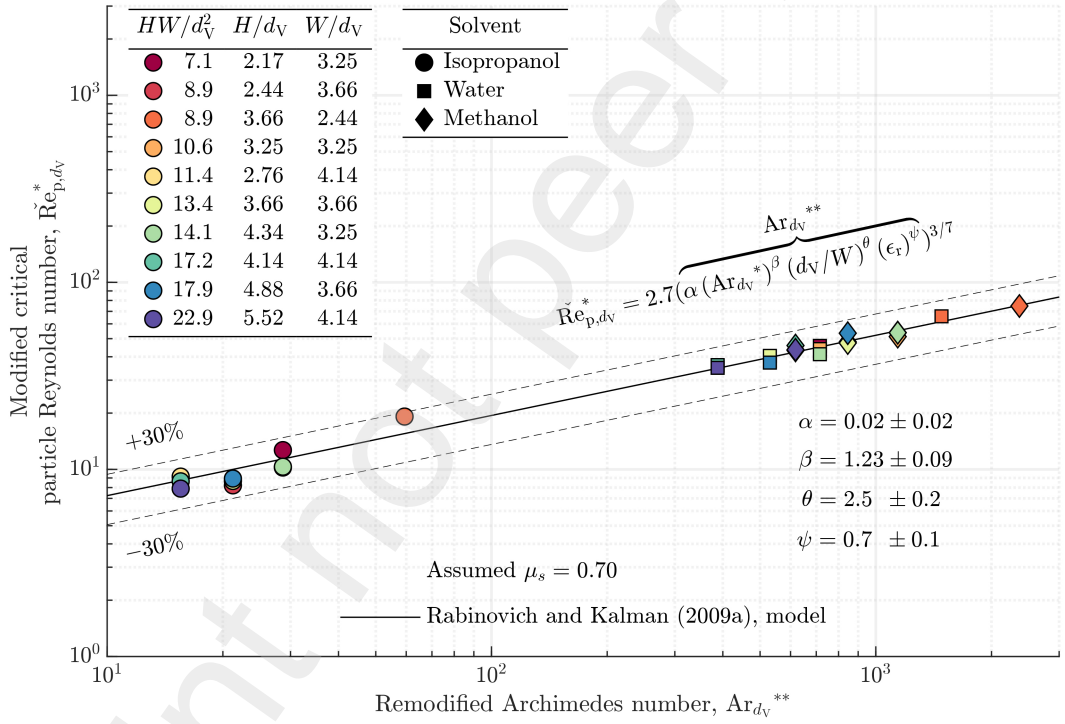

Highlights

Characterization of the critical lift-off of a single flat-plate microchip particle in straight rectangular microchannel flows

Raymond Yeung, Cynthia Sainz, Jason Mandala, Philip Brisk, William H. Grover, Victor G. J. Rodgers

- Characterization accounts for entrance and electrostatic effects on critical lift-off
- Channel dimensions (H, W) and particle diameter (D) significantly affect lift-off
- Solvent dielectric constant (ϵ_r) found to be a significant factor affecting lift-off
- Empirical model, considering W, D, ϵ_r, provides excellent prediction for lift-off

Characterization of the critical lift-off of a single flat-plate microchip particle in straight rectangular microchannel flows

Raymond Yeung[a], Cynthia Sainz[b], Jason Mandala[c], Philip Brisk[d], William H. Grover[a], Victor G. J. Rodgers[a,*]

[a]*Department of Bioengineering, University of California, Riverside, Riverside, 92521, CA, USA*
[b]*Department of Evolution, Ecology, and Organismal Biology, University of California, Riverside, Riverside, 92521, CA, USA*
[c]*Department of Electrical and Computer Engineering, University of California, Riverside, Riverside, 92521, CA, USA*
[d]*Department of Computer Science and Engineering, University of California, Riverside, Riverside, 92521, CA, USA*

Abstract

Hydrodynamic sorting of microchip particles in microchannels is essential in microfluidic systems used for applications requiring particle-based multiplexing. Understanding the forces acting on a microchip in a microchannel, as well as the dependencies of the forces on channel and fluid flow parameters, allows for prediction of the flow conditions needed to initiate particle movement, or lift-off. This study presents the experimental characterization of the lift-off of a single, flat-plate, non-neutrally buoyant microchip particle initially sedimented near the inlet of straight, rectangular microfluidic channels of different channel sizes and solvents. The critical shear Reynolds number, corresponding to the minimum required for lift-off, was found to increase in particulate flow systems with larger Archimedes number. For channel aspect ratios $H/W \neq 1$, as the ratio of the channel area over the particle rotational diameter squared, HW/d_{max}^2, increased, the observed critical shear Reynolds number decreased. The observed lift-off for the flat-plate particle deviated from that predicted using a previous generalized critical lift-off model based on the modified Reynolds and Archimedes numbers. Numerical evaluations of the hydrodynamic forces acting on the particle revealed that electrostatic forces are significant. A remodified Archimedes number, based on the channel width, particle diameter, and solvent relative permittivity, is introduced as a correction to the generalized lift-off model to account for hydrodynamics and electrostatics affecting the lift-off of a flat-plate particle. Our model is in good agreement with the generalized particle lift-off model and allows for prediction of flat-plate particle lift-off in microfluidic channels.

Keywords: Lift-off, critical, pickup, microfluidic, particle, non-spherical

1. Introduction

Lift-off, the initiation of motion and suspension of sedimented solid particles through hydrodynamic interactions from the surrounding fluid, is a key process for the transport of non-neutrally buoyant particles flowing in microchannels. Microfluidics has emerged as a preferred method for particle manipulation due to the continued advancements in microchannel fabrication and understanding of particulate microchannel flow dynamics in microchannels. Among the particle manipulation techniques used in microfluidic systems, such as acoustic, electrophoretic, and magnetic methods, hydrodynamics is widely used on its own due to the advantage of offering passive lateral and axial positioning of particles simply from controlling the operating fluid flow and channel dimensions (Amini et al., 2014). The optimal design and operation of microfluidics used for hydrodynamic particle manipulation and sorting depends upon the understanding of the channel and fluid parameters affecting lift-off, and the prediction of the minimum operating flow conditions necessary for particle entrainment.

There has been increasing interest in incorporating silicon-based, non-neutrally buoyant microchip particles into microfluidic systems for a variety of applications involving particle manipulation. Flat-plate, silicon microchips, which may be fabricated with ease and at scale from patterning and dicing of silicon wafers, have emerged as key particles to transport in microfluidic systems for screening (Hoffmann et al., 2007a,b) and combinatorial synthesis (Vastl et al., 2017; Xiao et al., 2000). For applications requiring microparticle encoding for multiplexed detections and reactions, microchips offer increased reliability of patterning and significantly greater number of unique encoding combinations over other microparticles (Li et al., 2010). Moreover, the surface of silicon microchips may be functionalized for tailored applications (Birtwell and Morgan, 2009; Li et al., 2010, 2015). Flat-plate, silicon microparticles used in microfluidics have included microbarcodes that are optically encoded (Cunin et al., 2002; Eun Chung et al., 2009; Hoffmann et al., 2006, 2007b; Jensen-McMullin et al., 2008) and also microtransponders that store codes in memory and transmit the codes using radio frequency (Mandecki et al., 2006).

However, there is a lack in understanding of the particulate flow behavior, including lift-off, of these non-spherical, non-neutrally buoyant microparticles in microfluidic channels.

*Corresponding author
Email address: victor.rodgers@ucr.edu (Victor G. J. Rodgers)

Therefore, an investigation of the channel configurations and fluid parameters affecting lift-off of flat-plate, non-neutrally buoyant microparticles in microchannels is needed to develop a model to predict the minimum operating flow conditions for hydrodynamic-induced movement of this subset of particles in different microfluidic particulate flow systems.

Initiation of particle movement through pneumatic conveying (PC) and hydraulic conveying (HC) has been practiced for well over a century and significant work has been performed in the last several decades to develop a methodology to determine the flow conditions necessary for suspension of both a single particle, and multiple particles from a sedimented particulate layer. Many terms are used in literature to refer to the threshold, or minimum, tangential fluid flow conditions for suspension of sedimented particles during horizontal conveying: pickup (gas in pipes), wind (gas in large tunnels), critical (liquid in pipes and channels), lift-off (liquid in Poiseuille flow), and detachment (liquid in cylindrical microchannel; or air through a plug). For clarity, these terms for suspension differ from saltation in relation to the initial position of the particles. Suspension involves particles initially at rest and sedimented at the bottom of the fluidic conduit whereas for saltation, the particles are initially suspended.

Moreover, there are many different parameters used in both empirical and theoretical models to describe the fluid flow for particle suspension. The threshold fluid velocity is typically expressed in terms of the average fluid velocity, $\langle U \rangle$, or maximum fluid velocity, $U_{\max}$. However, the shear velocity, $U_* = \sqrt{\tau/\rho_f}$, where τ is the shear stress at an arbitrary fluid layer and ρ_f is the fluid density, is also extensively used in theoretical models since the threshold shear velocity represents the fluid velocity profile around the particle and wall boundary. Several dimensionless numbers have been developed to derive generalized models for different conveying systems. The parameters affecting the vertical flow have been described using the Froude number (Fr), the square root of the ratio of the inertial force and the particle weight, and the Archimedes number (Ar), the square of the ratio of the gravitational force and viscous force. While Fr is found to be valid for PC systems (Cabrejos and Klinzing, 1992, 1994), it neglects the buoyancy force and has been found to be invalid for HC systems. The Archimedes number, which captures the effect of buoyancy, has been demonstrated to be more appropriate for analysis of both PC (Kalman et al., 2005; Rabinovich and Kalman, 2007) and HC (Rabinovich and Kalman, 2007, 2008, 2009a,b) systems. The parameters affecting the horizontal flow, which is dominated by the inertial force and opposing viscous force, have been described using the Reynolds number (Re), particle Reynolds number ($\mathrm{Re_p}$), and shear Reynolds number ($\mathrm{Re_s}$), in relation to the channel, particle, and shear flow, respectively (Patankar et al., 2001; Kalman, 2022).

Extensive experimental and computational work have been performed towards predicting the critical fluid flow conditions for suspension of particles in channels (25 to 150 mm in diameter) for horizontally-oriented HC processes. Kalman and Rabinovich gathered experimental data from various studies to develop a generalized empirical model to predict the threshold $\mathrm{Re_p}$ for particle suspension as a function of Ar (Kalman et al., 2005; Rabinovich and Kalman, 2007, 2008, 2009a,b). Critical suspension is dependent on many factors including the fluid density, number of particles (single or layer of particles), channel diameter, particle shape, and particle friction coefficient. Rabinovich and Kalman (2009a) compiled experimental data from studies on the incipient motion of a single particle in air (Halow, 1973; Cabrejos and Klinzing, 1992; Stevenson et al., 2002; Hubert and Kalman, 2004; Rabinovich and Kalman, 2009a) and water (Han and Hunt, 1995) in horizontal particulate flow systems. They proposed a generalized relationship, which accounted for the effect of the channel diameter and particle friction coefficient, to predict the critical $\mathrm{Re_p}$ for lift-off of a single particle as a function of Ar.

Only a few studies have investigated the threshold flow conditions for particle suspension in microchannels. Direct numerical simulation of a single spherical particle in planar Poiseuille flow through a rectangular microchannel using an arbitrary Lagrangian-Eulerian (ALE) method indicated that the critical shear Reynolds number for particle lift-off decreases as the ratio of the channel height and the particle rotational diameter, $H/d_{\max}$, also referred to as the height domain size, increases (Patankar et al., 2001). The simulation data could be represented by power law equations for each $H/d_{\max}$. In another work, from experimental studies of the lift-off of spherical particles in cylindrical microchannel flows, the detachment fluid velocity was found to decrease as the ratio of the channel diameter and the particle rotational diameter, $D/d_{\max}$, increases (Shukla and Henthorn, 2009). Although the previous works provided initial key insights regarding the effects of the channel-particle size on critical lift-off of particles in microchannels, the studies ignore both entrance and electrostatic effects on lift-off.

In this study, we experimentally investigated the hydrodynamic lift-off of a single sedimented flat-plate, non-neutrally buoyant microchip particle in straight, horizontally-aligned, rectangular cross-section microchannels. Using different combinations of solvents (isopropyl alcohol, water, and methanol) and microchannels of different cross-sectional sizes, we examined the effects of the solvent kinematic viscosity and channel dimensions on the critical shear Reynolds number for lift-off. Through dimensional analysis and comparison of our data on critical lift-off of flat-plate particles to that of spherical particles from previous studies, we re-examined the use of the channel-particle size parameter, typically defined as $H/d_{\max}$, in expressing the dependency of the critical shear Reynolds number on the particle-channel size. We proposed and demonstrated that both the ratio of the channel area over the particle rotational diameter squared, $HW/d_{\max}^2$, also referred to as the area domain size, as well as the channel aspect ratio, $AR = H/W$, are needed for prediction of flat-plate particle lift-off in rectangular microchannels. While many previous lift-off studies place particles near the middle of the channel length to eliminate entrance and end effects in the analysis, practical particle sorting applications typically involve preloading particles towards a physical particle mesh or trap integrated

into the microfluidic system. Moreover, electrostatic effects on lift-off are often eliminated in experimental particulate flow characterization systems through the use of antistatic sprays or nonionic surfactants. In consideration of pragmatic applications, we performed experimental particle lift-off studies with the microchip particle beginning at rest near a physical particle trap upstream of each rectangular microchannel. Towards assessing the effect of the trap and the positioning of the particle at the inlet on the observed particle lift-off, we performed computational fluid dynamics (CFD) simulations of a stationary particle at various locations along the channel length, and evaluated the drag, lift, and electrostatic adhesion forces acting on the particle. In efforts to verify and improve empirical models for critical lift-off of particles in microfluidic channels, we mapped our single flat-plate particle lift-off data to a previously developed generalized curve for prediction of lift-off in horizontal particulate flow systems. We introduced a remodified Archimedes number, which accounts for the lift-off dependency on particle-channel size and electrostatic adhesion, to develop an empirical model for accurate prediction of lift-off of microchip and other flat-plate particles in a variety of microfluidic particulate flow systems.

2. Modeling approaches

2.1. Dimensionless numbers

For our analysis, we considered the channel Reynolds number, particle Reynolds, and shear Reynolds number to capture parameters affecting horizontal fluid flow, and the Archimedes number to describe parameters affecting the vertical fluid flow. The dimensionless numbers for the analysis of lift-off in horizontal hydraulic conveying in microchannels include:

$$\mathrm{Re} = \frac{\rho_\mathrm{f}\langle U\rangle D_\mathrm{H}}{\mu} \qquad \text{channel Reynolds number} \qquad (1)$$

$$\mathrm{Re}_{\mathrm{p},d} = \left(\frac{d}{D_\mathrm{H}}\right)^2 \mathrm{Re} \qquad \text{particle Reynolds number} \qquad (2)$$

$$\mathrm{Re}_{\mathrm{s},d} = \frac{\rho_\mathrm{f}\langle\dot{\gamma}_\mathrm{w}\rangle d^2}{\mu} \qquad \text{shear Reynolds number} \qquad (3)$$

$$\mathrm{Ar}_d = \frac{\rho_\mathrm{f}(\rho_\mathrm{p}-\rho_\mathrm{f})gd^3}{\mu^2} \qquad \text{Archimedes number} \qquad (4)$$

where ρ_f is the fluid density, $\langle U\rangle$ is the average fluid velocity, D_H is the channel hydraulic diameter, μ is the fluid dynamic viscosity, d is the characteristic particle diameter, $\langle\dot{\gamma}_\mathrm{w}\rangle$ is the average shear rate at the bottom channel wall, ρ_p is the particle density, and g is the standard acceleration of gravity. To compare our experimental lift-off data to that from other studies that use different definitions to describe the size of the non-spherical particle, we considered both commonly used definitions of d: the particle rotational diameter, d_max, and the equivalent volume spherical particle diameter, d_V. For our study of a square prism, flat-plate particle (consisting of a height of h, and a square base with an edge width of w), the rotational diameter is defined as $d_\mathrm{max} = w\sqrt{2}$ and the equivalent volume spherical particle diameter is defined as $d_\mathrm{V} = (6hw^2/\pi)^{1/3}$. It is noted that the critical velocity, used in the evaluation of Eq. (1) and Eq. (3), is the superficial velocity, the flow velocity evaluated with only the fluid present.

2.2. Models of single particle lift-off in horizontal flow systems

Patankar et al. (2001) performed 2-D direct numerical simulations of the lift-off of a single spherical particle in planar Poiseuille flow. They observed that the critical shear Reynolds number, $\check{\mathrm{Re}}_{\mathrm{s},d_\mathrm{max}}$, for lift-off at a given Archimedes number, $\mathrm{Ar}_{d_\mathrm{max}}$, decreases as H/d_max increases; an asymptotic value for $\check{\mathrm{Re}}_{\mathrm{s},d_\mathrm{max}}$ is reached above a certain H/d_max. An empirical relationship between $\check{\mathrm{Re}}_{\mathrm{s},d_\mathrm{max}}$ and $\mathrm{Ar}_{d_\mathrm{max}}$ at a specified H/d_max may be described using a power law equation:

$$\mathrm{Ar}_{d_\mathrm{max}} = a\left(\check{\mathrm{Re}}_{\mathrm{s},d_\mathrm{max}}\right)^b \qquad (5)$$

where a and b are fitted parameters for each H/d_max.

In related work, Kalman and Rabinovich conducted particle lift-off experiments and compiled experimental data from other works to generate a generalized curve for threshold suspension in different particulate flow systems (Kalman et al., 2005; Rabinovich and Kalman, 2007, 2008, 2009a). From the hundreds of experiments collected, a power law relationship between the $\check{\mathrm{Re}}_{\mathrm{p},d_\mathrm{V}}$ and $\mathrm{Ar}_{d_\mathrm{V}}$ effectively described the data with over 90% of the experiments within ± 30% error:

$$\frac{\check{\mathrm{Re}}_{\mathrm{p},d_\mathrm{V}}}{r} = c(\mathrm{Ar}_{d_\mathrm{V}}k)^m \qquad (6)$$

where r is a parameter adjusting $\check{\mathrm{Re}}_{\mathrm{p},d_\mathrm{V}}$ to account for different channel sizes used in the experiments, c is an empirical parameter, k is a parameter adjusting $\mathrm{Ar}_{d_\mathrm{V}}$ by an additional effect based on particle properties (particle sphericity, ϕ, or static friction coefficient, μ_sf), and m is an empirical power term. The parameters used in Eq. (6) are dependent on various factors, including, but not limited to, the type of threshold process (suspension or saltation), number of particles (single particle or a layer of particles), medium of fluid (gas or liquid), defining the particulate flow conditions of the studied system.

For the remaining discussion, the dimensionless parameters presented will be those corresponding to that from an empirical expression for the critical lift-off of a single particle from a rectangular channel in liquid flow adapted from Rabinovich and Kalman (2009a). A modified critical particle Reynolds number, $\check{\mathrm{Re}}^*_{\mathrm{p},d_\mathrm{V}} = \check{\mathrm{Re}}_{\mathrm{p},d_\mathrm{V}}/r$, is defined such that for rectangular channels, each with a hydraulic diameter $D_\mathrm{H} = (2HW/(H+W))$, the measured critical average velocities may be converted to that for a reference 50 mm diameter (D_{50}) cylindrical pipe using an exponentially bounded function:

$$\check{\mathrm{Re}}^*_{\mathrm{p},d_\mathrm{V}} = \frac{\check{\mathrm{Re}}_{\mathrm{p},d_\mathrm{V}}}{(1.25 - 0.5\exp(-(D_\mathrm{H}/D_{50})/1.5))} \qquad (7)$$

It is noted that D_H in Eq. (7) has replaced D, defined as the diameter of a cylindrical pipe or as the channel width W for experiments involving a square duct, from the original

expression for incipient motion of a single particle in liquid channels formulated by Rabinovich and Kalman (2009a).

To account for the effect of friction between the particle and channel wall, Rabinovich and Kalman (2009a) proposed a modified Archimedes number, $\mathrm{Ar}^*_{d_\mathrm{V}} = \mathrm{Ar}_{d_\mathrm{V}} k$, also defined as:

$$\mathrm{Ar}^*_{d_\mathrm{V}} = \mathrm{Ar}_{d_\mathrm{V}} \mu_\mathrm{sf} \tag{8}$$

where μ_sf is the static particle-wall friction coefficient.

Based on experiments of individual large particles ($d > 0.4$ mm) in both pneumatic and hydraulic conveying systems, Rabinovich and Kalman (2009a) determined the following relationship for the critical lift-off of a single particle from a channel in liquid flow:

$$\check{\mathrm{Re}}^*_{\mathrm{p},d_\mathrm{V}} = 2.7 \mathrm{Ar}^{*\,3/7}_{d_\mathrm{V}} \qquad 8000 < \mathrm{Ar}^*_{d_\mathrm{V}} < 8.7 \times 10^6 \tag{9}$$

2.3. Forces acting on a single flat-plate particle

Fig. 1 shows the dominant forces acting on a single flat-plate particle initially sedimented on the bottom wall of a rectangular duct in Poiseuille flow. The forces may be categorized into those acting parallel (horizontal) to the wall and those acting perpendicular (vertical) to the wall. The summation of the dominant horizontal forces is given by:

$$\sum \mathbf{F}_x = \mathbf{F}_\mathrm{D} - \mathbf{F}_\mathrm{F} \tag{10}$$

where $\mathbf{F}_\mathrm{D}$ is the drag force and $\mathbf{F}_\mathrm{F}$ is the friction force. The summation of the dominant vertical forces is given by:

$$\sum \mathbf{F}_y = \mathbf{F}_\mathrm{L} + \mathbf{F}_\mathrm{B} - \mathbf{F}_\mathrm{G} - \mathbf{F}_\mathrm{A} \tag{11}$$

where $\mathbf{F}_\mathrm{L}$ is the lift force, $\mathbf{F}_\mathrm{B}$ is the buoyancy force, $\mathbf{F}_\mathrm{G}$ is the gravity force, and $\mathbf{F}_\mathrm{A}$ is the adhesion force.

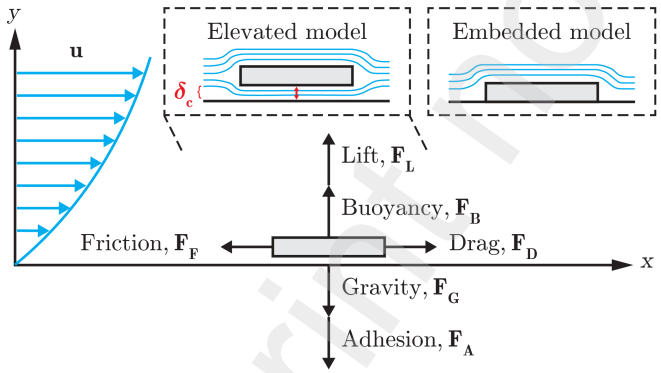

Figure 1: Forces acting on a single flat-plate particle in Poiseuille flow through a rectangular duct. Encouraging forces to initiate particle motion and suspension include lift, buoyancy, and drag while resisting forces include gravity, adhesion, and friction. Accurate evaluations of drag and lift forces acting on the particle were made using computational simulations with an elevated model that provides a clearance, δ_c, between the particle and the wall boundary.

There are two potential modes of incipient motion for a non-spherical, flat-plate particle from rest: sliding or lifting (Hubbe, 1984; Rabinovich and Kalman, 2009b). The sliding mechanism occurs when the drag force overcomes the friction force. The lifting mechanism starts when the lift and buoyancy forces overcome the gravity and adhesion forces. The mode responsible for the incipient motion is the one for which the encouraging forces ($\mathbf{F}_\mathrm{D}$, $\mathbf{F}_\mathrm{L}$, $\mathbf{F}_\mathrm{B}$) are greater than the resisting forces ($\mathbf{F}_\mathrm{F}$, $\mathbf{F}_\mathrm{G}$, $\mathbf{F}_\mathrm{A}$) at the lowest fluid velocity. The adhesion forces include van der Waals and electrostatic forces. The van der Waals forces have been shown to be negligible for larger particles (Cabrejos and Klinzing, 1992).

2.4. Particle clearance with an elevated model

When employing numerical methods to evaluate the forces acting on a particle near a wall, appropriate placement of the particle needs to be considered. For numerical simulations of the flow around a moving particle with a moving fluidic mesh, contact of the particle and wall may pose convergence issues due to the topology change (Patankar et al., 2001). Even for numerical studies of the flow around a stationary particle with a stationary fluidic mesh, the particle-wall contact may lead to issues due to the singularity at the point of contact. Previous studies on lift of a spherical particle from a flat surface in shear flow highlighted problems in the evaluation of lift due to the singularity at the contact point leading to local inaccuracies of the evaluated stresses (Krishnan and Leighton Jr, 1995). As shown in Fig. 1, there are two general approaches for appropriate particle placement to address the problems of particle-wall contact: an embedded model and an elevated model. Embedding the particle at different depths into the wall has been investigated in attempts to address the issue of the singularity at the contact point for a spherical particle (Martinez et al., 2009). However, the embedded model may provided a negative evaluated lift force due to the removal of the bottom particle surface where the pressure component of the lift force acts in the upward direction (Palakurthi et al., 2017). Alternatively, another approach involves providing a clearance distance, δ_c, between the particle and wall. The limiting case of a particle in contact with the wall can be approached by progressively decreasing δ_c (Leighton and Acrivos, 1985; Cherukat and Mclaughlin, 1994). However, small values for δ_c requires sufficiently high discretization for accurate computation of the flow field and stresses on the particle (Zeng et al., 2009; Lee and Balachandar, 2017).

2.5. Analytical solution of the average wall shear rate for flow through a finite rectangular channel

For characterization of the critical shear Reynolds number for hydrodynamic particle lift-off in rectangular microchannels, we evaluated the analytical solution of the average wall shear rate along the bottom surface of a channel, with channel height H, channel width W, and channel length L, in the absence of a particle. The fluid velocity profile along the x-direction, $U_x(y,z)$, has been previously derived for laminar flow of an incompressible, Newtonian fluid through a finite rectangular channel (Truskey et al., 2004):

$$U_x(y,z) = \frac{\Delta p H^2}{8\mu L}\left[\left(1 - \frac{4y^2}{H^2}\right) - \sum_{n=0}^{\infty} \frac{32(-1)^n \cosh\left((2n+1)\pi z/H\right)\cos\left((2n+1)\pi y/H\right)}{(2n+1)^3\pi^3 \cosh\left((2n+1)\pi W/2H\right)}\right] \tag{12}$$

where Δp is the pressure drop and μ is the fluid dynamic viscosity. The average wall shear rate along the bottom surface at $y = -H/2$ may then be calculated:

$$\langle \dot{\gamma}_w \rangle = \frac{\tau_{yx}}{\mu} = \frac{1}{W}\int_{-W/2}^{W/2}\left(\frac{\partial U_x}{\partial y}\bigg|_{y=-H/2}\right)dz = \frac{\Delta p H}{2\mu L}\left[1 - 16\left(\frac{H}{W}\right)\sum_{n=0}^{\infty}\frac{(-1)^n \tanh\left((2n+1)\pi W/(2H)\right)}{(2n+1)^3\pi^3}\right] \tag{13}$$

where τ_{yx} is the shear stress in the x-direction acting on the surface with its outward normal vector in the y-direction. The average wall shear rate in Eq. (13) is dependent on the pressure drop, Δp, but we can reexpress $\langle \dot{\gamma}_w \rangle$ as a function of the fluid flow rate, Q. The fluid flow rate is given by:

$$Q = 4\int_0^{W/2}\int_0^{H/2} U_x(y,z)\,dy\,dz \tag{14}$$

Following substitution, the average wall shear rate, which is used for evaluating the shear Reynolds number, may then be calculated using the following expression:

$$\langle \dot{\gamma}_w \rangle = \left(\frac{6Q}{H^2 W}\right)\left[1 - 6\left(\frac{H}{W}\right)\sum_{n=0}^{\infty}\frac{\tanh\left((2n+1)\pi W/2H\right)}{(2n+1)^5\pi^5}\right]^{-1} \left[1 - 16\left(\frac{H}{W}\right)\sum_{n=0}^{\infty}\frac{(-1)^n \tanh\left((2n+1)\pi W/2H\right)}{(2n+1)^3\pi^3}\right] \tag{15}$$

3. Experimental methods

3.1. Dimensional analysis

An aim of the current study is to determine the fluid and channel variables affecting the critical lift-off mechanism of flat-plate, non-neutrally buoyant particles in horizontal channels with a rectangular cross-section:

$$f\left(d, \rho_p, H, W, D_H, \mu, \rho_f, \langle U \rangle, \langle \dot{\gamma}_w \rangle, g\right) = 0 \tag{16}$$

where the functional relationship f must be independent of a specific system of units (Gibbings, 2011). Through nondimensionalization using the Buckingham π theorem (Buckingham, 1914; Karam and Saad, 2021), the above expression may be restated as a relationship F, in terms of dimensionless π groups, that may describe the lift-off mechanism of flat-plate particles in horizontal channels with a rectangular cross-section:

$$F\left(\frac{H}{d}, \frac{W}{d}, \frac{d}{D_H}, \frac{\rho_p}{\rho_f}, \frac{\rho_p{}^2 g d^3}{\mu}, \frac{\rho_f \langle U \rangle D_H}{\mu}, \frac{\rho_f \langle \dot{\gamma}_w \rangle d^2}{\mu}\right) = 0 \tag{17}$$

where the sixth π group is the channel Reynolds number and the seventh π group is the shear Reynolds number. It can be observed that the third and sixth π groups may be manipulated to provide the particle Reynolds number. Also, through manipulation of the fourth and fifth π groups, the Archimedes number may be found. While dimensional analysis revealed the potential significance of the channel-particle size parameters, H/d and W/d, in affecting the particle lift-off, the two π groups may also be manipulated to account for the possibility of the channel cross-sectional area, $A = HW$, and the aspect ratio (H/W) also being significant parameters. From application of dimensional analysis, the critical shear Reynolds number, $\check{\mathrm{Re}}_{s,d}$, necessary for lift-off of a single flat-plate particle in horizontal, rectangular channels, may then be formulated to be be dependent on the following parameters:

$$\check{\mathrm{Re}}_{s,d} = F\left(\frac{H}{d}, \frac{W}{d}, \frac{HW}{d^2}, \frac{H}{W}, Ar_d, Re, Re_{p,d}\right) \tag{18}$$

3.2. Particle and fluids

A p-Chip (p-Chip Corporation, Chicago, IL, USA), a 600 μm × 600 μm × 100 μm microtransponder, was used as a representative flat-plate, non-neutrally buoyant microchip particle for the single particle lift-off studies. The properties of p-Chips have been previously described by Mandecki et al. (Gruda et al., 2010; Li et al., 2010; Lin et al., 2007; Mandecki et al., 2006; Rich et al., 2012). The p-Chip is a non-uniform, composite object fabricated using a planar semiconductor manufacturing process from silicon wafers that have been deposited and patterned with layers of polysilicon and silicon dioxide, and diced into individual microchips. However, since the deposited layers are relatively thin compared to the thickness of the underlying silicon, we consider the p-Chip as a uniform particle with properties of silicon for our analysis. Also, one of the major surfaces of the p-Chip contains integrated circuits, microfeatures that may affect the friction along the surface. From inclined plane tests, we determined that the difference between the particle-wall kinetic friction coefficients, μ_{kf}, with respect to the two major particle surfaces was insignificant (Supplementary Material Section S1). As a result, the non-uniformity of the surfaces of the p-Chip has a negligible effect on the observed flow conditions for particle lift-off. Based on previous studies of non-spherical sand of the same size range as the p-Chip, we assumed the value of 0.70 for the static friction coefficient, μ_{sf}, between the particle and wall (Rabinovich and Kalman, 2009a) for the calculation of the modified Archimedes number in Eq. (8). Isopropyl alcohol, deionized water, and methanol (Sigma-Aldrich, St. Louis, MO, USA), each with different kinematic viscosities, were chosen as solvents for the particulate flow studies. The physical properties of the particle and fluids are summarized in Table 1.

Table 1
Physical properties of the flat-plate particle and fluids for particulate microchannel flow studies at 25°C.

	Material	Density, ρ (kg/m^3)	Dynamic viscosity, μ (Pa s)	Relative permittivity, ϵ_r (-)
Solid particle	p-Chip	2329	-	-
Fluid phase	Isopropyl alcohol	785	2.07×10^{-3}	78.39
	Water	997	8.89×10^{-4}	19.92
	Methanol	792	5.40×10^{-4}	32.70

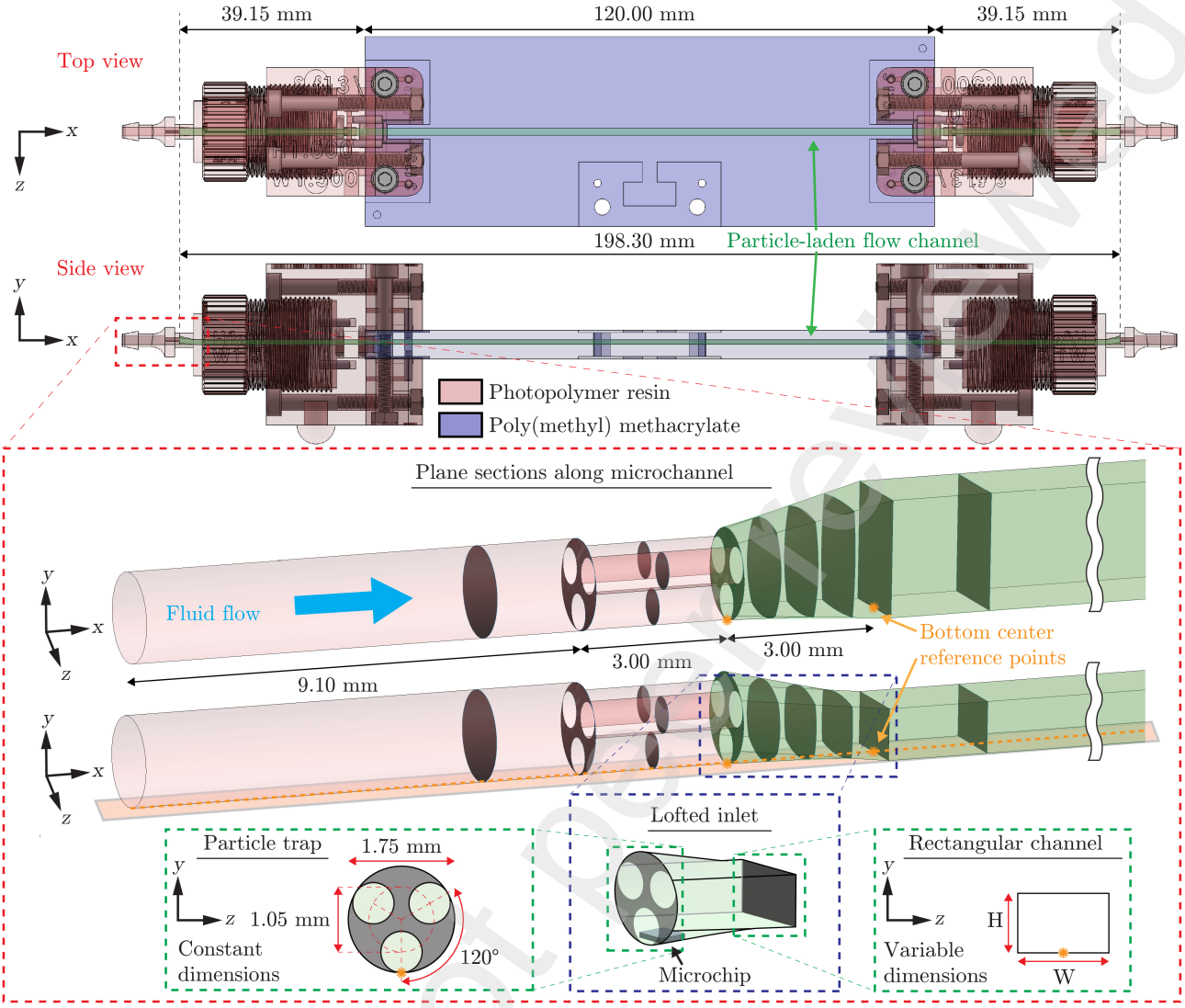

Figure 2: Design of the straight rectangular microchannel device for experimental particulate flow studies of lift-off of a single flat-plate microchip particle sedimented at the inlet near a physical particle trap containing three through holes. Experimental lift-off fluid flow rates were assessed for all combinations of fluid solvents, and channel configurations with different channel areas and aspect ratios.

3.3. Channel fabrication and experimental setup

A 3^2 central composite face-centered (CCF) design with replicated center points was used to construct the design of experiments outlining the configurations for the rectangular channel, with different channel heights (H) and channel widths (W) used for the particulate flow studies. Three levels were chosen for each of the two factors considered: channel aspect ratio, H/W, and width domain size, W/d_{max}. An additional experimental design point (H: 1.50 mm, W: 1.00 mm) was added to investigate the effect of the channel aspect ratio on the critical lift-off behavior. Table 2 presents all the channel configurations used in the current experimental and computational lift-off studies. The dimensions presented in the study are the dimensionally accurate values ± 0.03 mm.

The design and features of the microfluidic manifold are illustrated in in Fig. 2. Designs of microfluidic channels were created in the vector graphics software, Adobe Illustrator 2023 (Adobe Inc., San Jose, CA). To fabricate the chip, we machined poly(methyl methacrylate) (PMMA) sheets using a desktop computer numerical control (CNC) mill (Bantam Tools Desktop PCB Milling Machine, Peekskill, NY, USA). The PMMA sheets were sealed to form the rectangular microchannels using an ethanol-assisted thermal bonding process (Liga et al., 2016). Custom fluidic adapters with an integrated physical particle trap were designed using SOLIDWORKS 2022 (Dassault Systèmes, Waltham, MA, USA) and 3-D printed using the Form 3B stereolithography printer with Formlabs Clear v04 resin (Formlabs, Somerville, MA, USA). The fine features of the device were fabricated at the resolution of 25 µm for both the CNC mill and 3-D printer. A fluidic adapter was directly interfaced to both the inlet and outlet of the PMMA microchannel to allow for horizontal fluid flow delivery to the microfluidic device while keeping the microchip particle contained within the manifold. Viton™

Table 2
Experimental configurations for the microchannels with rectangular cross-sections.

Experimental characterization						
	Channel dimensions (mm)		Channel aspect ratio (-)	Channel-particle domain size parameters (-)		
Configuration	H	W	H/W	W/d_{max}	H/d_{max}	HW/d_{max}^2
1	1.00	1.50	0.67	1.77	1.18	2.08
2	1.50	1.00	1.50	1.18	1.77	2.08
3	1.50	1.50	1.00	1.77	1.77	3.13
4	0.89	1.33	0.67	1.57	1.05	1.65
5	1.33	1.33	1.00	1.57	1.57	2.47
6	1.13	1.70	0.67	2.00	1.33	2.67
7	2.26	1.70	1.33	2.00	2.67	5.30
8	1.78	1.33	1.33	1.57	2.09	3.29
9	2.00	1.50	1.33	1.77	2.36	4.20
10	1.70	1.70	1.00	2.00	2.00	4.00

fluoroelastomer O-rings (The Chemours Company, Wilmington, DE, USA) were added in between conduit interfaces to achieve a fluidic seal. A horizontally-oriented fluidic adapter, with the inlet parallel to the channel length, was chosen over a perpendicular interconnection to eliminate corner vortices that could indefinitely trap the particle. The design of the physical particle trap, which had a circular cross-section containing three equally-spaced circular through holes (0.7 mm in diameter) in a radial pattern, allowed for sufficient resin clearance during component fabrication and also facilitated flow stabilization during the particulate flow experiments. The size and orientation of the circular cross-section of the particle trap were held constant for all tested channel configurations. The bottom point of the circular surface of the trap was coincident with the bottom channel plane. The circular surface of the particle trap was lofted to the rectangular surface of the channel for each experimental configuration. The nominal channel length was 200 mm.

Fig. 3 shows the experimental assembly for the particulate flow experiments to evaluate the critical flow rates for microchip particle lift-off. Alignment of the microfluidic manifold was maintained using integrated Maxwell kinematic couplings between the device adapters and the base mount (Slocum, 2010). Fluid was delivered to the microchannel at set constant flow rates using a syringe pump (Model 44, Harvard Apparatus, Holliston, MA USA). The syringe pump, connected to a computer through an RS-232 interface, was controlled using a custom LabVIEW virtual instrument (VI) program (NI LabVIEW 2020, Austin, TX, USA). A top-mounted, USB 3.0, 1.3 MP, monochrome camera (MQ013MG-ON, Ximea, Münster, Germany) with an attached lens configuration (MVL6X12Z, MVL20A, MVLCMC, MVL6X025L, MVL05A; Thorlabs, Newton, NJ, USA) was used to capture video recordings (at 1500 frames per second) of the particle motion along the xz-plane coincident with the channel width and channel length. A 10K lux LED panel was mounted at the bottom of the transparent microfluidic channel to provide uniform lighting and achieve fast image acquisition. The field of view of the camera encompasses the transparent PMMA microfluidic channel downstream of the translucent particle trap inlet.

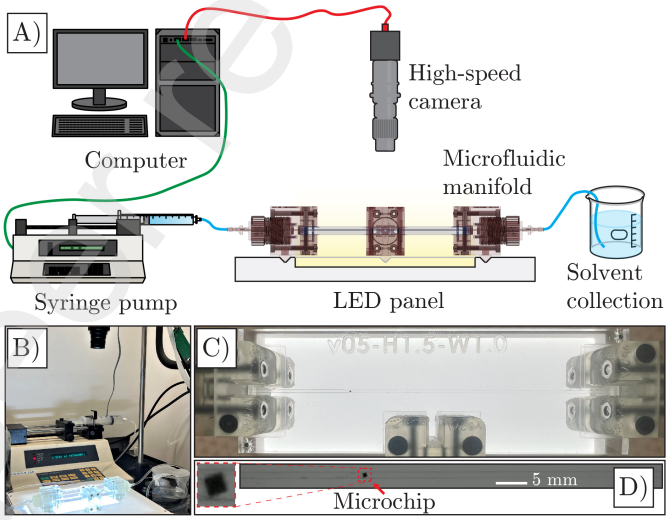

Figure 3: Experimental assembly for the characterization of microchip particle lift-off. A) Schematic of the assembly for characterizing the lift-off of a single flat-plate particle initially sedimented near the inlet of a microfluidic channel. The minimum flow rate for lift-off of the particle was recorded for each of the experimental configurations with different channel and solvent combinations. B) Camera image of the experimental particulate flow setup. C) Top-down camera image of an illuminated channel from a specific configuration (H = 1.50 mm, W = 1.00 mm). D) Full frame from a recorded video (H = 1.50 mm, W = 1.00 mm, Q = 7 mL/min) of the flowing microchip particle.

3.4. *Particle lift-off experiments*

A single p-Chip was loaded into the microfluidic manifold and encapsulated between the particle traps. A programmed sequence from the LabVIEW VI was used to flow the single p-Chip, at a specified constant flow rate and at room temperature of 25 °C, in a forward-backward cycle with a brief pause between each state transition to allow sufficient time for the flow system to stabilize and for the p-Chip to settle near the inlet particle trap prior to collection of lift-off data. Videos of the flowing p-Chip, initially sedimented on the bottom channel adjacent to the inlet particle trap, were collected at various constant fluid flow rates. For each experimental configuration with a particular solvent, channel design, and specified constant fluid flow rate, five experimental trials were performed to determine the critical volumetric flow rate

necessary for lift-off. The critical flow rate for particle lift-off at each experimental configuration was defined to be the flow rate (probed at 1 mL/min steps) necessary for steady particle movement among all five experimental trials. The experiments were performed for all combinations of solvents (isopropyl alcohol, water, and methanol) and channel configurations defined in Table 2. The data was analyzed using MATLAB 2023a (MathWorks, Natick, MA, USA).

4. Computational methods

4.1. Numerical models of single particle microchannel flow

To gain insight into the hydrodynamic forces acting on the flat-plate particle at the experimentally observed critical fluid flow rates for particle lift-off and to assess the effects of the particle trap on the hydrodynamic forces acting on the particle, we performed CFD simulations of the steady-state fluid flow around a single, stationary, sedimented, flat-plate particle located near the bottom channel wall and at different lengths along the axial channel centerline. The present study uses a finite element method implemented using the COMSOL Multiphysics® software with the CFD Module (COMSOL, Inc., Burlington, MA, USA) to numerically solve the continuity and Navier-Stokes equations for a laminar flow model of an incompressible, Newtonian fluid of constant density. Since we are investigating the forces leading to the incipient motion of a particle initially at rest, a stationary solver is used to resolve the steady-state flow. Also, the simulations consider only the fluid domain; the solid particle is modeled as a void volume within the fluid domain. The fluid flow around a single particle sedimented on the bottom wall boundary is more appropriately expressed using an elevated model that positions the particle at an elevated location with a vertical clearance distance between the particle and wall to account for stresses on the bottom surface of the particle (Palakurthi et al., 2017). Therefore, we specified a clearance distance of δ_c between the particle and the channel wall.

4.2. Governing equations

The steady-state laminar flow of an incompressible, Newtonian fluid with an external gravity force in the negative y-direction was modeled using the following forms of the Navier-Stokes and continuity equations, respectively:

$$\rho_f(\mathbf{u}\cdot\nabla)\mathbf{u} = \nabla\cdot\boldsymbol{\sigma} + \rho_f\mathbf{g} \tag{19}$$

$$\rho_f\nabla\cdot\mathbf{u} = 0 \tag{20}$$

where ρ_f is the fluid density, $\mathbf{u}$ is the fluid velocity vector, and $\mathbf{g}$ is the gravitational field. The total stress tensor, $\boldsymbol{\sigma}$, is composed of the pressure component, $-p\mathbf{I}$, and viscous stress tensor, $\boldsymbol{\tau}$:

$$\boldsymbol{\sigma} = -p\mathbf{I} + \boldsymbol{\tau} \tag{21}$$

where p is the pressure and $\mathbf{I}$ is the identity matrix. The viscous stress tensor, $\boldsymbol{\tau}$, is given by:

$$\boldsymbol{\tau} = \mu_f\left(\nabla\mathbf{u} + (\nabla\mathbf{u})^T\right) \tag{22}$$

where μ_f is the dynamic viscosity of the fluid and T is the tranpose. The forces acting on the particle are evaluated by integrating the total stress contributions around the entire particle surface, S. The drag force, which considers all the tangent, x-directional stresses, and the lift force, composed of the normal, y-directional stresses, may then be evaluated by:

$$\mathbf{F}_D = \int_S \mathbf{n}_x\cdot\boldsymbol{\sigma}\, dS \tag{23}$$

$$\mathbf{F}_L = \int_S \mathbf{n}_y\cdot\boldsymbol{\sigma}\, dS \tag{24}$$

where $\mathbf{n}_x$ and $\mathbf{n}_y$ are the outward unit normal in the x-direction and y-direction, respectively.

4.3. Computational domain, boundary conditions, and mesh

Since the experimental characterization of lift-off of a single flat-plate particle was performed with the particle at rest near the inlet consisting of a lofted particle trap, the entrance effects on lift-off needed to be investigated. To evaluate the hydrodynamic forces acting on the particle to initiate lift-off, we performed computational simulations using the fluidic domain of each configuration of the particle trap adapter where the particle initially begins at rest. The distance from the particle trap cross-section to the outlet of the computational domain was 33.18 mm. Since the channel exhibits symmetry about the xy-plane, we performed CFD simulations on half of the full channel geometry. A constant flow rate corresponding to half of the experimentally observed critical flow rate needed for lift-off was applied as the inlet boundary condition. A constant atmospheric pressure boundary condition was set at the outlet. The no-slip boundary condition was applied for all the walls and particle surfaces. The reported values for the evaluated drag and lift forces correspond to that acting on a full (non-halved) particle. Free tetradehedral mesh elements were used for the fluidic domain and hexahedral mesh elements with further mesh refinement are used for the boundary layers.

For some configurations, the entrance length $L_e = 0.058D_H\mathrm{Re}$ (Bergman, 2011) beyond which the flow is fully developed, was estimated to be greater than the length of the computational domain of the imported channel adapter. As a result, fully-developed models with a stationary particle situated in the middle of a 2 mm length channel were also performed to evaluate the hydrodynamic forces downstream.

An assessment of an appropriate mesh configuration and a bottom clearance distance, δ_c, was performed to provide accurate numerical evaluations of the forces acting on the particle. A mesh independence study was performed in terms of the evaluated drag and lift forces to ensure that the numerical solutions for the hydrodynamic forces do not change significantly with further mesh refinement. The configurations for the mesh considered in the mesh independence study included minimum boundary element sizes ranging from 637 μm to 2.55 μm. Comparison of the results from successive mesh designs with minimum boundary element sizes, $e_{nb,min}$, of 19 μm and 51 μm yieled relative errors of 2.7% and 6.2% for the evaluated drag and lift forces,

respectively. Therefore, the mesh configuration with $e_{nb,min}$ of 51 µm was used for all simulations. For the evaluation of an appropriate distance for the bottom clearance between the particle and the bottom channel wall, results were compared for simulation configurations with clearance distances, δ_c, of 0.01, 0.05, and 0.1 mm. Through comparison of the evaluated hydrodynamic forces from successive δ_c considered, the clearance distance of 0.05 mm was determined to be sufficient for evaluation of the forces with relative errors of 1.8% and 7.8% for the drag and lift forces, respectively. While further refinement in both the mesh and clearance distance was possible for some experimental channel and solvent configurations, certain cases yielded convergence issues related to the sliver faces and other small features. The main parameters used in the simulations are summarized in Table 3.

Table 3
Parameters used for computational simulations of a single, stationary flat-plate particle in straight rectangular microchannel flows.

Numerical simulation		
Parameter	**Definition**	**Value(s)**
δ_c	Clearance between bottom of particle and bottom channel wall (mm)	0.05
ΔL_p	Axial distance of particle from inlet (mm)	0.10, 0.90, 2.40, 3.01, 23.00
$e_{ng,max}$	Global maximum element size (mm)	0.854
$e_{ng,min}$	Global minimum element size (mm)	0.255
$e_{nb,max}$	Boundary maximum element size (mm)	0.471
$e_{nb,min}$	Boundary minimum element size (mm)	0.051
e_{num}	Average number of elements	73 900 ± 600

4.4. Parametric computational studies and particle positioning

Preparation of the computational particulate flow simulations included several requirements: 1) construction of parametric geometries corresponding to the different microchannels investigated, 2) configurable placement of the particle at various distances from the bottom channel wall and from the channel inlet, and 3) precise positioning of the flat-plate particle in relation to the complex geometry of the particle trap containing curved, lofted walls. Therefore, we used SOLIDWORKS to construct the designs of the channel configurations and define configurable relations between the particle and channel features, the LiveLink™ for SOLIDWORKS module (COMSOL, Inc., Burlington, MA, USA) to import the configurable parameters into COMSOL, and COMSOL to perform the parametric particulate flow simulations for all channel and fluid flow configurations.

Computer-aided design of each microchannel was prepared as a configuration within SOLIDWORKS. The orientation of the particle was constrained such that the particle *xy*-midplane, located between two minor surfaces of the flat-plate particle, remained coincident with the channel *xy*-midplane situated between the side channel walls. For precise orientation of the flat-plate particle in relation to the inlet as well as the bottom channel wall, several reference lines were mounted on the particle. The particle distance, ΔL_p, the axial distance between the particle and inlet, is defined by the length of an outward reference line that is perpendicular to the minor surface of the particle. The endpoints of this reference line are coincident to the centroid of the minor particle surface and the channel inlet surface, respectively. The bottom clearance, δ_c, the distance between the bottom, major surface of the particle and the bottom channel wall, is defined as the length of outward reference lines that are perpendicular to the major particle surface. These reference lines originate from the corners of the major particle surface and the other endpoints of the lines are coincident with the bottom channel wall. Fig. 4 shows the computational domain, boundary conditions, mesh, and particle positioning for a specific configuration (H = 1.00 mm, W = 1.50 mm, δ_c = 0.05 mm, ΔL_p = 0.90 mm).

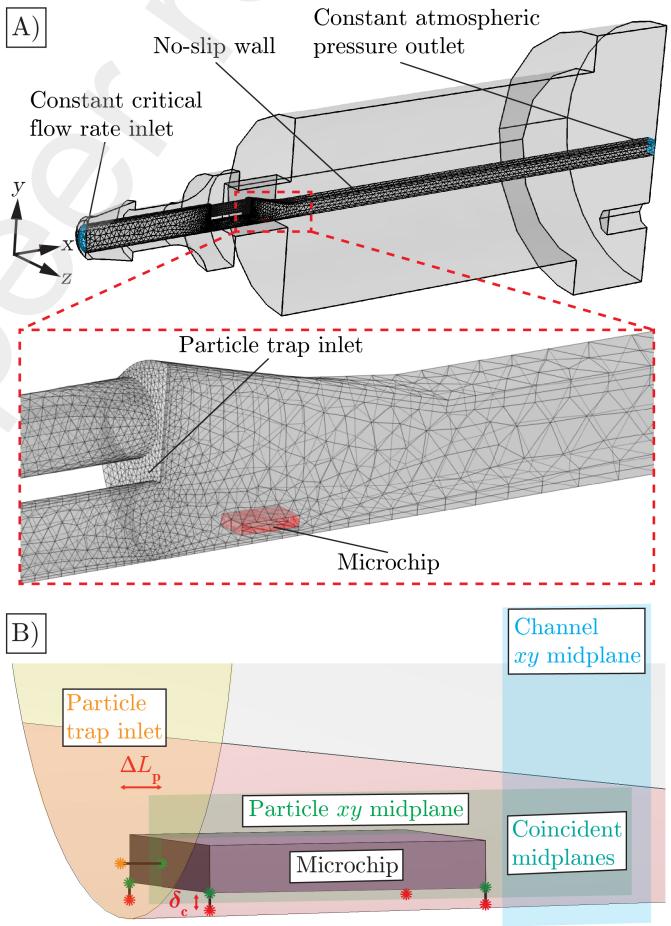

Figure 4: Computational domain, boundary conditions, mesh, and particle position for the numerical simulations to evaluate the hydrodynamic drag and lift forces acting on a single flat-plate microchip particle initially sedimented near the microchannel inlet. The channel configuration shown corresponds to that for H = 1.00 mm, W = 1.50 mm, δ_c = 0.05 mm, ΔL_p = 0.90 mm. A) Computational fluid domain corresponding to a halved model of the particle trap adapter containing a pseudo-particle modeled as a void volume. B) Schematic of the positioning of the particle in the simulations with the following configurable parameters: the axial distance of the particle from the inlet, ΔL_p, and clearance distance between the bottom particle surface and the bottom channel wall, δ_c.

5. Results and Discussion

5.1. Experimental flat-plate particle lift-off

Fig. 5 and Fig. 6 present the observed critical shear Reynolds number, $\check{\mathrm{Re}}_{s,d_{\max}}$, as a function of the Archimedes number, $\mathrm{Ar}_{d_{\max}}$, for all ten channel configurations and three solvents tested. The results for a flat-plate particle with $\mathrm{Ar}_{d_{\max}}$ ranging from 1695 to 25020 were compared to that from a separate numerical study for a spherical particle with $\mathrm{Ar}_{d_{\max}}$ ranging from 2 to 6363 (Patankar et al., 2001). It is noted that the different $\mathrm{Ar}_{d_{\max}}$ reported for the current particle lift-off studies for a flat-plate particle reflect only the changes in the solvent properties since a single type of particle was considered in the study. As was observed from previous findings for a spherical particle, it is observed that greater $\check{\mathrm{Re}}_{s,d_{\max}}$ is required to lift the flat-plate particle at higher $\mathrm{Ar}_{d_{\max}}$.

At each $\mathrm{Ar}_{d_{\max}}$ considered in the experimental particulate flow studies for a flat-plate particle, an increase in the height domain size, $H/d_{\max}$, resulted in a lower $\check{\mathrm{Re}}_{s,d_{\max}}$ for lift-off. Patankar et al. (2001) showed that the $\check{\mathrm{Re}}_{s,d_{\max}}$ for a spherical particle at different $\mathrm{Ar}_{d_{\max}}$ may be modeled using an empirical power law equation for each $H/d_{\max}$ considered. Fig. 5 shows the $\check{\mathrm{Re}}_{s,d_{\max}}$ for a flat-plate particle at different $\mathrm{Ar}_{d_{\max}}$ and $H/d_{\max}$ are within the range of values from the extrapolated power law equations from Patankar et al. (2001). However, the values of $H/d_{\max}$ for a flat-plate particle were significantly lower than that for a spherical particle for the relationship between $\check{\mathrm{Re}}_{s,d_{\max}}$ and $\mathrm{Ar}_{d_{\max}}$. A flat-plate particle at rest may experience both incipient lifting and sliding motion but a spherical particle may also experience an additional rolling motion, so the range of $H/d_{\max}$ values for the relationship between $\check{\mathrm{Re}}_{s,d_{\max}}$ and $\mathrm{Ar}_{d_{\max}}$ was expected to be lower for a flat-plate particle. We also observed the experimentally characterized relationship between $\check{\mathrm{Re}}_{s,d_{\max}}$ and $\mathrm{Ar}_{d_{\max}}$ for the flat-plate particle deviated from the power law models formulated from numerical simulations for a spherical particle (Patankar et al., 2001). Since the previous numerical simulations from Patankar et al. (2001) did not account for adhesion forces, the deviations from the present study suggest that for this relatively large microchip particle, electrostatic adhesion forces may significantly affect the lift-off behavior.

In addition, the area domain size, $HW/d_{\max}^2$, which was determined through dimensional analysis to be a potential channel-particle size parameter affecting $\check{\mathrm{Re}}_{s,d_{\max}}$, was shown to be a more appropriate parameter than $H/d_{\max}$ (Patankar et al., 2001; Hur et al., 2011) to capture the effects of the channel-particle size in three-dimensions. The comparison of the lift-off for a flat-plate particle and a spherical particle

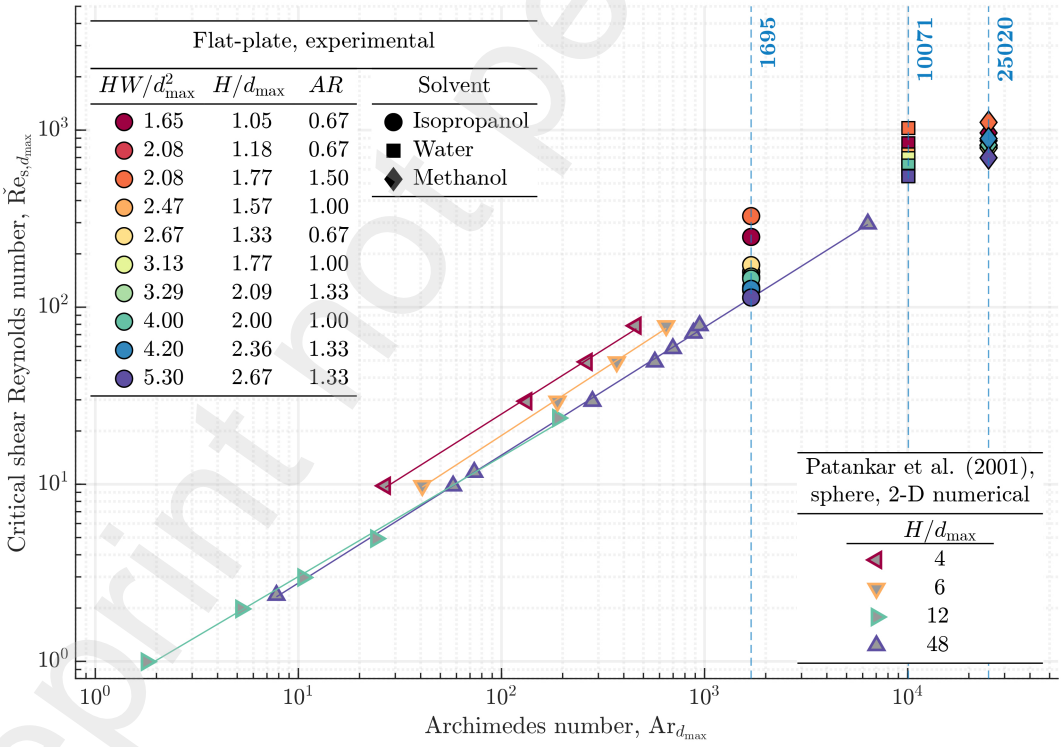

Figure 5: Effect of the Archimedes number, $\mathrm{Ar}_{d_{\max}}$, and channel-particle domain sizes, $H/d_{\max}$ and $HW/d_{\max}^2$, on the critical shear Reynolds, $\check{\mathrm{Re}}_{s,d_{\max}}$, for particle lift-off. The experimental data for lift-off of a flat-plate particle is compared to 2-D ALE numerical data for lift-off of a spherical particle (Patankar et al., 2001). The range of values for $H/d_{\max}$ needed for lift-off of a flat-plate particle is significantly lower than that evaluated from planar numerical studies for a spherical particle, suggesting relationships for lift-off of a spherical particle may not be directly applied to an aspherical, flat-plate particle without additional corrections. Both the height domain size, $H/d_{\max}$, and the area domain size, $HW/d_{\max}^2$, affects $\check{\mathrm{Re}}_{s,d_{\max}}$. However, $HW/d_{\max}^2$ appropriately captures the 3-D contributions of the channel dimensions to the flow profile around the particle. While the relationship between $\mathrm{Ar}_{d_{\max}}$ and $\check{\mathrm{Re}}_{s,d_{\max}}$ for a spherical particle was previously determined to follow an empirical power law model for each channel-particle domain size, it is noted that the current flat-plate particle lift-off data deviates from the extrapolated linear relationships. The deviation suggests electrostatic effects, which are not considered in the previous ALE study, significantly affect lift-off.

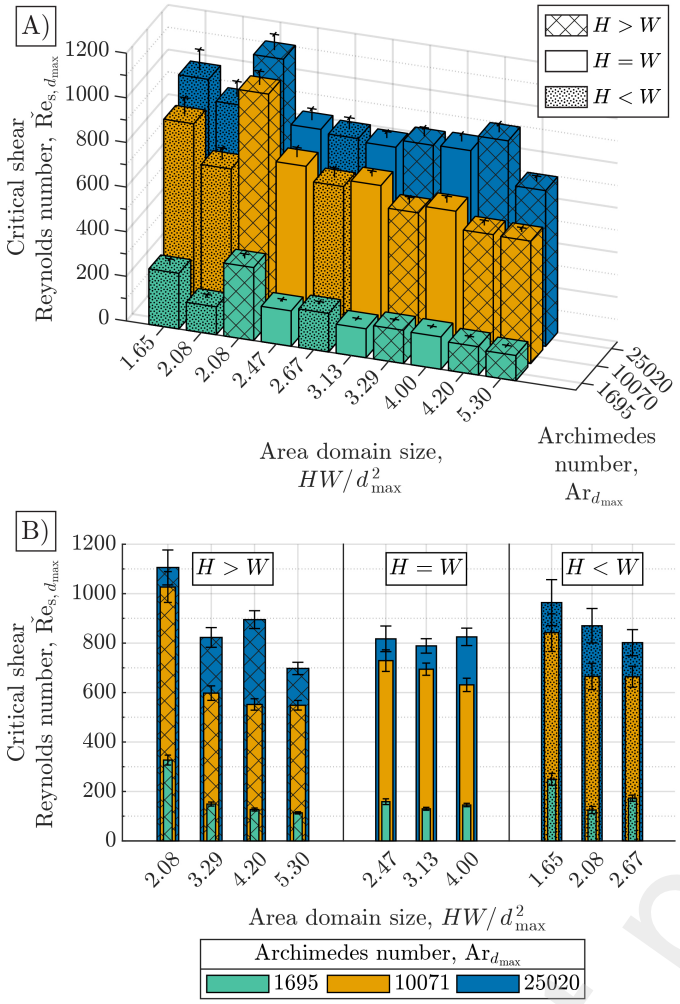

Figure 6: Experimentally characterized lift-off of a flat-plate particle at different Archimedes number, $\mathrm{Ar}_{d_{max}}$, area domain sizes, HW/d^2_{max}, and channel aspect ratios, H/W. A) The critical shear Reynolds number, $\check{\mathrm{Re}}_{s,d_{max}}$, as a function of HW/d^2_{max} and $\mathrm{Ar}_{d_{max}}$. At each $\mathrm{Ar}_{d_{max}}$, higher HW/d^2_{max} generally reduced the $\check{\mathrm{Re}}_{s,d_{max}}$, but HW/d^2_{max} alone cannot accurately predict $\check{\mathrm{Re}}_{s,d_{max}}$. B) Effect of HW/d^2_{max} and $\mathrm{Ar}_{d_{max}}$ at different H/W. At each considered $\mathrm{Ar}_{d_{max}}$, an increase in HW/d^2_{max} resulted in a decrease in $\check{\mathrm{Re}}_{s,d_{max}}$ for $H/W \neq 1$. For $H/W = 1$, changes in HW/d^2_{max} did not significantly affect the observed $\check{\mathrm{Re}}_{s,d_{max}}$.

revealed similarities in the lift-off behavior but also showed that characterization studies and models for lift-off of spherical particles cannot be used to accurately predict the lift-off of non-spherical, flat-plate particles. It is noted that although the lift-off results are discussed with respect to HW/d^2_{max} and H/d_{max}, these results effectively reflect only the effect of the channel dimensions on lift-off since d_{max} remains constant for the single type of flat-plate particle considered.

In Fig. 6, the experimental data for $\check{\mathrm{Re}}_{s,d_{max}}$ and $\mathrm{Ar}_{d_{max}}$ was categorized in terms of the channel aspect ratio, H/W. We observed at each investigated $\mathrm{Ar}_{d_{max}}$ that an increase in HW/d^2_{max} resulted in a decrease in $\check{\mathrm{Re}}_{s,d_{max}}$ for $H/W \neq 1$. For $H/W = 1$, changes in HW/d^2_{max} did not significantly affect the observed $\check{\mathrm{Re}}_{s,d_{max}}$. The findings revealed that accurate prediction of $\check{\mathrm{Re}}_{s,d_{max}}$ at each $\mathrm{Ar}_{d_{max}}$ must consider both the area domain size, HW/d^2_{max}, and the channel aspect ratio, H/W.

5.2. *Simulation of hydrodynamic forces on particle*

Fig. 7 shows the computational particulate flow domain and numerically evaluated velocity profile around the stationary particle for one configuration (H = 1.00 mm, W = 1.50 mm, δ_c = 0.05 mm, ΔL_p = 0.90 mm) from the steady-state CFD studies. Both embedded and elevated particle models were investigated in the numerical simulations for evaluating the hydrodynamic forces. However, similar to previous findings from studies of spherical particle detachment (Palakurthi et al., 2017), an embedded flat-plate particle model yielded unrealistic, negative magnitudes for the evaluated lift forces. Evaluation of the forces on each of the six particle surfaces revealed that the lift forces acting on the particle are dominated by the pressure contributions to the top and bottom surfaces. As shown from the velocity profiles with streamlines around the particle, the current model using an elevated particle appropriately resolves the contributions of the forces acting on the bottom surface.

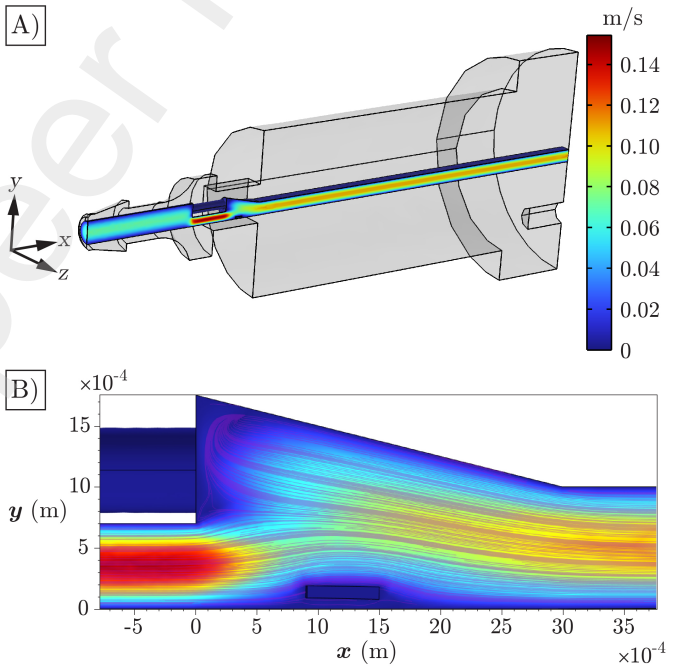

Figure 7: Numerically evaluated velocity profile with streamlines along the fluidic adapter and around the stationary particle for one of the channel configurations (H = 1.00 mm, W = 1.50 mm, δ_c = 0.05 mm, ΔL_p = 0.90 mm). A) 3-D fluid velocity profile through the fluidic domain of the fluidic adapter. B) xy-view of the fluid velocity profile with streamlines around the particle. The steady-state CFD study with the elevated particle appropriately considered the contributions of the stresses on the bottom surface of the particle to the total hydrodynamic forces acting on the particle.

Fig. 8 presents the evaluated lift forces acting on the flat-plate particle from the fully-developed CFD studies with a stationary particle positioned at various axial distances along the channel. The data is categorized and presented in terms of the different configurations of the channel aspect ratio (H/W) and the solvent. For all configurations investigated, the flat-plate particle experienced elevated lift forces at the region near the inlet particle trap. However, as the particle was

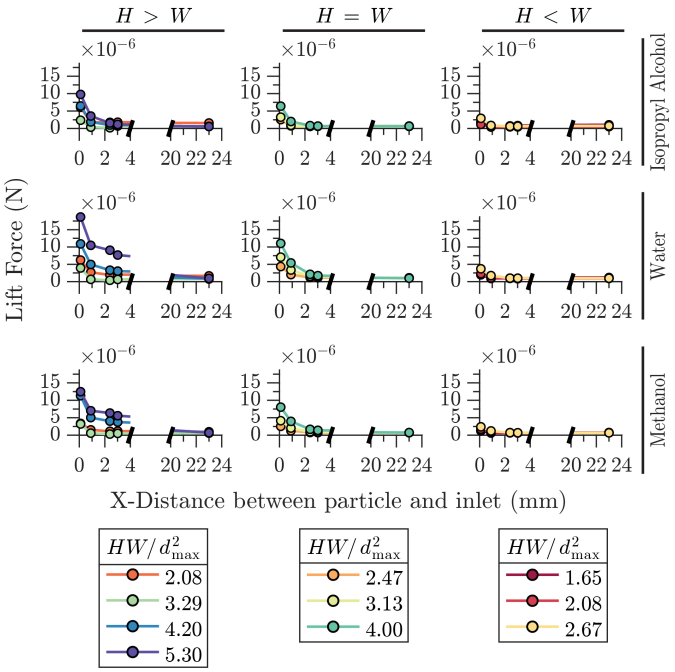

Figure 8: Evaluated lift forces acting on the flat-plate particle from steady-state computational models with a stationary particle at various axial distances along the channel. The evaluated forces are shown for different configurations of channel aspect ratios (H/W) and solvent. The particle experienced elevated lift forces along the entrance of the inlet particle trap. However, the magnitudes of the lift forces evaluated with the particle downstream for all experimental configurations showed a strong convergence towards a singular value of $(6.7 \pm 0.4) \times 10^{-8}$ N indicating the particle remained suspended after lift-off.

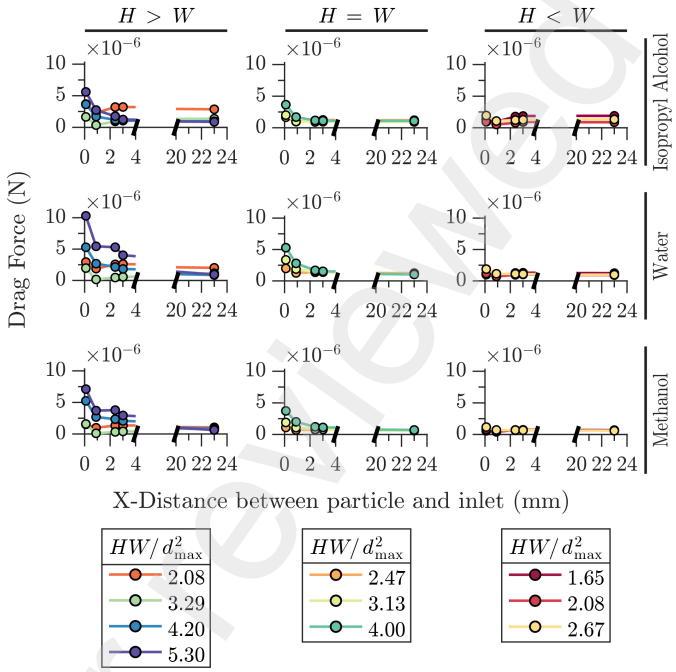

Figure 9: Evaluated drag forces acting on the flat-plate particle from steady-state computational models with a stationary particle at various axial distances along the channel. The evaluated forces are shown for different configurations of channel aspect ratios (H/W) and solvent. The flat-plate particle generally experiences elevated drag forces along the entrance of the inlet particle trap. The magnitudes of the drag forces evaluated with the particle downstream for all experimental configurations do not all converge to a single value suggesting the particle does not slide along the bottom channel after lift-off.

positioned further downstream, the magnitudes of the lift forces decayed. Interestingly, for all configurations of the computational studies, which employ the experimentally observed critical flow rates for flat-plate particle lift-off as a constant inlet boundary condition, the lift forces converged to a singular value of $(6.7 \pm 0.4) \times 10^{-7}$ N when the particle was positioned beyond the entrance length, L_e. While the results are insufficient for determining whether the incipient motion of the particle from rest begins with sliding or lifting, the findings reveal the particle remains suspended during saltation, or following initial particle suspension.

The drag forces acting on the flat-plate particle, positioned along the channel length, were also evaluated and presented in Fig. 9. As was observed for the lift forces, the drag forces acting on the particle were elevated in the region near the inlet particle trap and decayed rapidly as the particle was positioned further along the channel length. However, evaluation of the drag forces with the particle positioned downstream of L_e presented a range of values from 5.9×10^{-7} to 2.9×10^{-6} N among all study configurations. The findings further indicate that following initial suspension, the transported particle remains suspended rather than sliding along the channel.

Although the CFD studies numerically resolved only the hydrodynamic forces on the particle, the electrostatic adhesion force was determined using the balance of the vertical forces, which include gravity, electrostatic, buoyant, and lift, acting on the particle positioned beyond L_e. The electrostatic adhesion force was determined to be 1.2×10^{-7} N, 2.0×10^{-7} N, and 1.3×10^{-7} N in isopropyl alcohol, water, and methanol, respectively. The electrostatic adhesion force was determined to be significant as it accounted for approximately 13 to 21 % of the total downward vertical force. Since electrostatics played a significant factor in affecting the observed particle lift-off, it must be considered in both analysis of the lift-off data and development of a predictive model for lift-off.

5.3. *Comparison of flat-plate lift-off data to generalized model*

Fig. 10 maps the current data on flat-plate particle lift-off to a generalized model for lift-off (Rabinovich and Kalman, 2009a) of various particulate flow systems based on a power law relationship between the modified critical particle Reynolds number, $\check{\mathrm{Re}}^*_{\mathrm{p},d_\mathrm{V}}$ (Eq. (7)), and the modified Archimedes number, $\mathrm{Ar}^*_{d_\mathrm{V}}$ (Eq. (8)). Although the flat-plate particle lift-off data was generally comparable to that predicted using the generalized model, notable deviations may be observed. First, every range of values of the observed $\check{\mathrm{Re}}^*_{\mathrm{p},d_\mathrm{V}}$ for a single flat-particle was significantly lower than the predicted $\check{\mathrm{Re}}^*_{\mathrm{p},d_\mathrm{V}}$ from the generalized model at each $\mathrm{Ar}^*_{d_\mathrm{V}}$ investigated. The reduction in the observed $\check{\mathrm{Re}}^*_{\mathrm{p},d_\mathrm{V}}$ compared to that predicted using the generalized model may be attributed to the enhanced lift and drag forces acting on the flat-plate particle at the entrance of the current particulate flow system. Second, our results revealed the significant contribution of the channel-particle size to the particle lift-off. Specifically, the

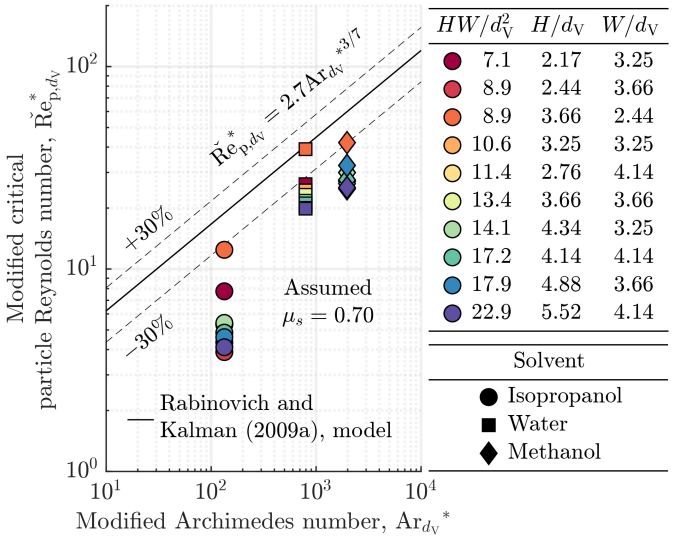

Figure 10: Experimental data for single flat-plate particle lift-off mapped onto a generalized curve (Rabinovich and Kalman, 2009a) for predicting particle lift-off in different particle-fluid systems. The particulate flow conditions needed for lift-off is presented as the modified critical particle Reynolds number, $\check{\mathrm{Re}}^*_{\mathrm{p},d_\mathrm{V}}$, which provided normalization for different channel hydraulic diameters, as a function of the modified Archimedes number, $\mathrm{Ar}^*_{d_\mathrm{V}}$, which accounted for the effect of friction between the particle and channel wall. Deviation of the data for a single flat-plate particle from the generalized lift-off model was attributed to the effects of the electrostatic forces, particle trap inlet, and channel-particle domain size on the particle lift-off.

adjustment of HW/d_V^2 from 1.65 to 5.30 resulted in changes in $\check{\mathrm{Re}}^*_{\mathrm{p},d_\mathrm{V}}$ by a factor of approximately 2 to 3. The large spread in $\check{\mathrm{Re}}^*_{\mathrm{p},d_\mathrm{V}}$ at various HW/d_V^2 indicated wall-effects have a tremendous effect on particle lift-off behavior, even more notably for microchannel particulate flow systems such as the one used in the present study, in which the ratio of the particle diameter to channel diameter, $d_\mathrm{V}/D_\mathrm{H}$, ranges from 0.2 to 0.4 compared to 8×10^{-3} to 2×10^{-4} for relatively large particulate flow systems considered by Rabinovich and Kalman (2009a). Third, the observed $\check{\mathrm{Re}}^*_{\mathrm{p},d_\mathrm{V}}$ as a function of $\mathrm{Ar}^*_{d_\mathrm{V}}$ at each HW/d_V^2 deviated from the linear power law relationship of the generalized model. While (Rabinovich and Kalman, 2009a) used antistatic spray on the active channel surfaces to preclude electrostatic effects, the current experimental work considered electrostatic effects and revealed electrostatic adhesion forces to be significant. The magnitude of electrostatic forces on particles have been shown to be sensitive to the relative permittivity, ϵ_r, of the solvent in which the particles are immersed in, with lower ϵ_r resulting in stronger electrostatic coupling (Stojimirović et al., 2020). The magnitudes of the differing electrostatic adhesion forces acting on the particle resolved in Subsection 5.2 are reflective of the different ϵ_r of the solvents (Table 1) and extent of electrostatic shielding. As a result, ϵ_r of the solvent must also be accounted for in particulate lift-off studies in which electrostatic effects are significant.

5.4. Correction to generalized lift-off model

A revision to the generalized lift-off model, with additional considerations of the effect of electrostatic, channel-particle size, and intrinsic properties of the particulate flow system, may be performed to predict the lift-off of a flat-plate particle in rectangular microchannel flows. As an initial model for prediction of lift-off of a flat-plate particle in rectangular microfluidic channels, a relationship between the critical particle Reynolds number and Archimedes number, similar to that from (Rabinovich and Kalman, 2009a), is proposed:

$$\check{\mathrm{Re}}^*_{\mathrm{p},d_\mathrm{V}} = 2.7\mathrm{Ar}^{**\,3/7}_{d_\mathrm{V}} \tag{25}$$

However, a remodified Archimedes number, $\mathrm{Ar}^{**}_{d_\mathrm{V}}$, is introduced to account for the effects of $\mathrm{Ar}^*_{d_\mathrm{V}}$, H/W, d_V/W, and ϵ_r with their respective empirical parameters, β, ξ, θ, ψ, and an additional α empirical modifier (Eq. (26)).

$$\mathrm{Ar}^{**}_{d_\mathrm{V}} = \alpha\,(\mathrm{Ar}_{d_\mathrm{V}}{}^*)^\beta\,(H/W)^\xi\,(d_\mathrm{V}/W)^\theta\,(\epsilon_\mathrm{r})^\psi \tag{26}$$

Nonlinear regression of the parameters was performed using a Levenberg-Marquardt least squares method (Levenberg, 1944; Marquardt, 1963). Although the effect of H, more specifically $HW/d^2_{\max}$ and H/W, on lift-off was shown to be locally significant at each investigated Archimedes number, the results of the nonlinear regression yielded $\xi \approx 1$, indicating that H/W was not necessary for prediction of $\check{\mathrm{Re}}^*_{\mathrm{p},d_\mathrm{V}}$ over a large range of $\mathrm{Ar}^{**}_{d_\mathrm{V}}$. Thus, a simplified correction to the Archimedes number is proposed (Eq. (27)):

$$\mathrm{Ar}^{**}_{d_\mathrm{V}} = \alpha\,(\mathrm{Ar}_{d_\mathrm{V}}{}^*)^\beta\,(d_\mathrm{V}/W)^\theta\,(\epsilon_\mathrm{r})^\psi \tag{27}$$

Fig. 11 shows the comparison of the current lift-off data for a flat-plate particle to the corrected generalized lift-off model based on the relationship between the modified critical particle Reynolds number, $\check{\mathrm{Re}}^*_{\mathrm{p},d_\mathrm{V}}$, and the remodified Archimedes number, $\mathrm{Ar}^{**}_{d_\mathrm{V}}$. The lift-off data fits well with the revised lift-off model for a flat-plate particle with a standard error of ± 0.8 and is within ± 30% of the model function.

6. Conclusions

The critical lift-off of a single flat-plate microchip particle in straight, horizontal, rectangular microchannels was investigated using both experimental characterization and numerical simulation studies. The channel-particle domain size, HW/d^2, and the channel aspect ratio, H/W, were determined to affect lift-off, as lower $\check{\mathrm{Re}}_{\mathrm{s},d_{\max}}$ was observed for higher HW/d^2 at each $\mathrm{Ar}_{d_{\max}}$ considered. From numerical particulate flow simulations, electrostatic adhesion forces acting on the particle were determined to be significant. Based on the experimental particulate flow studies, the critical particle Reynolds number as a function of a corrected Archimedes number, which accounted for the channel width, particle diameter, solvent relative permittivity, and intrinsic properties of the particulate flow system, was found to provide an excellent empirical correlation to predict the lift-off of a single flat-plate particle. The developed empirical model for

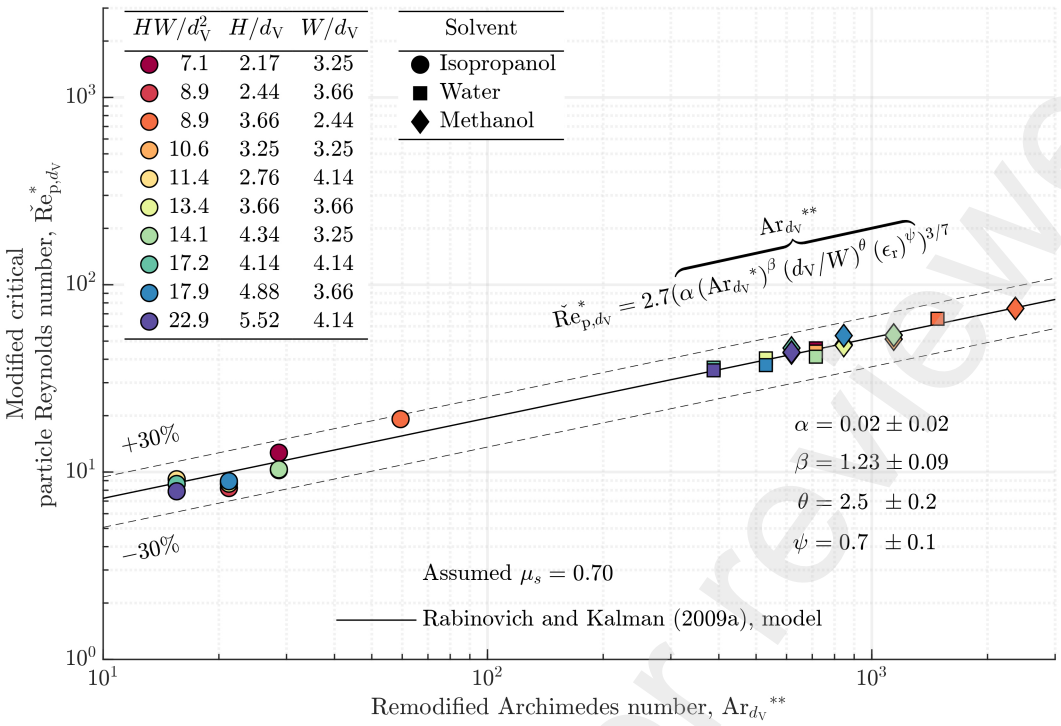

Figure 11: Experimental data for single flat-particle lift-off mapped onto a corrected generalized curve, adapted from a generalized particle lift-off model from Rabinovich and Kalman (2009a), using a remodified Archimedes number, $\mathrm{Ar}^{**}_{d_V}$, to account for the effects of the channel-particle domain size, relative permittivity of the solvent, and the particle trap inlet on the particle lift-off. Empirical parameters, α, β, θ, and ψ, for the current particulate flow system were evaluated from a nonlinear regression model. The corrected single flat-plate particle data using $\mathrm{Ar}^{**}_{d_V}$ is in good agreement with the generalized curve for prediction of particle lift-off in terms of the modified critical particle Reynolds number, $\check{\mathrm{Re}}^*_{p,d_V}$.

lift-off of a single microchip provides an accurate, first model for predicting the lift-off of a flat-plate particle under different microchannel and solvent configurations while accounting for entrance, wall, and electrostatic effects. The work provides a connection and knowledge transfer between the fields of pneumatic/hydraulic conveying and microfluidics towards furthering the understanding of particulate flow dynamics.

CRediT authorship contribution statement

Raymond Yeung: Conceptualization, Methodology, Formal Analysis, Investigation, Data Curation, Writing - Original Draft, Writing - Review & Editing, Visualization. **Cynthia Sainz:** Investigation, Data Curation. **Jason Mandala:** Software. **Philip Brisk:** Resources, Writing - Original Draft, Writing - Review & Editing, Supervision, Project Administration, Funding Acquisition. **William H. Grover:** Methodology, Formal Analysis, Resources, Writing - Original Draft, Writing - Review & Editing, Supervision, Project Administration, Funding Acquisition. **Victor G. J. Rodgers:** Conceptualization, Methodology, Formal Analysis, Resources, Writing - Original Draft, Writing - Review & Editing, Supervision, Project Administration, Funding Acquisition.

Declaration of competing interests

PB, WHG, and VGJR received a collaborative grant award (NSF CPS-1740052) with an industry collaborator, PharmaSeq, Inc., Monmouth, NJ (now p-Chip Corporation, Chicago, IL), who developed and provided microtransponders used for the study. PB, WHG, VGJR, RY, and JM were funded from the grant for the work performed in this study. The authors declare no additional competing interests.

Supplementary material

Supplementary material related to this article can be found online.

Data availability

Data will be made available on request.

Acknowledgments

This material is based upon work supported by the National Science Foundation under the Cyber-Physical Systems Award (Grant No. CPS-1740052), the Jacques S. Yeager, Sr. Professorship, and the University of California, Riverside Minigrant for Undergraduate Research and Creative Activities. We thank Richard Morris, Wlodek Mandecki, and Wesley Kopacka (p-Chip Corporation, Chicago, IL; formerly PharmaSeq, Inc., Monmouth Junction, NJ) for providing microtransponders and for their insightful discussions on microchip manipulation and sorting.

Nomenclature

Symbols

a	empirical parameter, Eq. (5)
A	channel cross-sectional area = HW (m^2)
AR	channel aspect ratio = H/W (m)
Ar_d	Archimedes number based on the characteristic particle diameter = $\rho_f(\rho_p - \rho_f)gd^3/\mu^2$ (-)
$\mathrm{Ar}_{d_{max}}$	Archimedes number based on particle rotational diameter = $\rho_f(\rho_p - \rho_f)gd_{max}^3/\mu^2$ (-)
Ar_{d_V}	Archimedes number based on equivalent volume spherical particle diameter = $\rho_f(\rho_p - \rho_f)gd_V^3/\mu^2$ (-)
$\mathrm{Ar}^*_{d_V}$	modified Archimedes number based on equivalent volume spherical particle diameter = $\mathrm{Ar}_{d_V}\mu_s$ (-)
b	empirical parameter, Eq. (5)
c	empirical parameter, Eq. (6)
d	characteristic particle diameter (m)
D	channel diameter (m)
D_{50}	reference 50 mm channel diameter (m)
D_H	channel hydraulic diameter (m)
d_{max}	particle rotational diameter (m)
d_V	equivalent volume spherical particle diameter (m)
$e_{nb,max}$	boundary maximum element size (m)
$e_{nb,min}$	boundary minimum element size (m)
$e_{ng,max}$	global maximum element size (m)
$e_{ng,min}$	global minimum element size (m)
$\mathbf{F}_A$	adhesion force (N)
$\mathbf{F}_B$	buoyant force = $\rho_f V_f g$ (N)
$\mathbf{F}_D$	drag force (N)
$\mathbf{F}_F$	friction force (N)
$\mathbf{F}_G$	gravity force = $-\rho_p V_p g$ (N)
$\mathbf{F}_L$	lift force (N)
Fr_d	Froude number based on characteristic particle diameter = $\langle U\rangle/\sqrt{gd}$ (-)
g	standard acceleration of gravity (m/s^2)
$\mathbf{g}$	gravitational field (m/s^2)
h	particle height (m)
H	channel height (m)
$\mathbf{I}$	identity matrix (-)
k	function of specific properties affecting the specific threshold suspension that adjusts the modified Archimedes number based on equivalent volume spherical particle diameter, Eq. (6)
L	channel length (m)
L_e	entrance length for rectangular channel = $0.058D_H\mathrm{Re}$ (m)
ΔL_p	axial distance of particle from inlet (m)
m	empirical power term, Eq. (6)
$\mathbf{n}_x$	outward unit normal vector in x-direction (-)
$\mathbf{n}_y$	outward unit normal vector in y-direction (-)
p	pressure (Pa)
Q	volumetric fluid flow rate (m^3/s)
$\check{Q}$	critical volumetric fluid flow rate for lift-off (m^3/s)
r	function of pipe diameter that adjusts the critical particle Reynolds number based on equivalent volume spherical particle diameter, Eq. (6)
Re	Reynolds number = $\rho_f\langle U\rangle D_H/\mu$ (-)
$\mathrm{Re}_{p,d}$	particle Reynolds number based on the characteristic particle diameter (-)
$\check{\mathrm{Re}}_{p,d_V}$	critical particle Reynolds number based on equivalent volume spherical particle diameter = $(d_V/D_H)^2\mathrm{Re}$ (-)
$\check{\mathrm{Re}}^*_{p,d_V}$	modified critical particle Reynolds number based on equivalent volume spherical particle diameter = $\mathrm{Re}_{p,d_V}/(1.25 - 0.5\exp((D_H/D_{50})/1.5))$ (-)
$\mathrm{Re}_{s,d}$	shear Reynolds number based on the characteristic particle diameter (-)
$\check{\mathrm{Re}}_{s,d_{max}}$	critical shear Reynolds number based on particle rotational diameter = $(d_{max}/D_H)^2\mathrm{Re}$ (-)
S	particle surface (m^2)
$\mathbf{u}$	fluid velocity vector (m/s)
U	superficial fluid velocity (m/s)
U_*	shear velocity (m/s)
$\langle U\rangle$	average fluid velocity (m/s)
U_{max}	maximum fluid velocity (m/s)
V_f	volume of displaced fluid (m^3)
V_p	volume of particle (m^3)
w	particle width (m)
W	channel width (m)

Greek Symbols

α	empirical multiplier for remodified Archimedes number, Eq. (26) and Eq. (27)
β	empirical power adjusting effect of modified Archimedes number, Eq. (26) and Eq. (27)
δ_c	clearance distance between particle and wall (m)
ϵ_r	relative permittivity or dielectric constant (-)
$\langle\dot{\gamma}_w\rangle$	average shear rate at the bottom channel wall (s^{-1})
μ	dynamic viscosity of fluid (Pa s)
μ_{kf}	kinetic friction coefficient between particle and wall (-)
μ_{sf}	static friction coefficient between particle and wall (-)
∇	del operator (m^{-1})
ϕ	particle sphericity, ratio of surface area of an equivalent volume sphere to the surface area of the particle (-)
ψ	empirical power adjusting effect of ϵ_r, Eq. (26) and Eq. (27)
ρ_f	density of fluid (kg/m^3)
ρ_p	density of particle (kg/m^3)
$\boldsymbol{\sigma}$	total stress tensor (Pa)
τ	shear stress (Pa)
$\boldsymbol{\tau}$	viscous stress tensor (Pa)
θ	empirical power adjusting effect of D/W, Eq. (26) and Eq. (27)
ξ	empirical power adjusting effect of H/W, Eq. (26)

Top Accents

$\check{}$	critical

Subscripts

A	adhesion

B	buoyant
D	drag
e	entrance
f	fluid
F	friction
G	gravity
H	hydraulic
kf	kinetic friction
L	lift
max	maximum
min	minimum
nb	numerical boundary
ng	numerical global
p	particle
r	relative
sf	static friction
s	shear
w	wall

Superscripts

*	modified
T	transpose

Abbreviations

ALE	arbitrary Lagrangian-Eulerian
CCF	central composite face-centered
CFD	computational fluid dynamics
CNC	computer numerical control
HC	hydraulic conveying
PC	pneumatic conveying
PMMA	poly(methyl methacrylate)

References

Amini, H., Lee, W., Carlo, D.D., 2014. Inertial microfluidic physics. Lab on a Chip 14, 2739–2761. URL: https://pubs.rsc.org/en/content/articlelanding/2014/lc/c4lc00128a, doi:10.1039/C4LC00128A. publisher: The Royal Society of Chemistry.

Bergman, T.L., 2011. Fundamentals of Heat and Mass Transfer. John Wiley & Sons. URL: https://www.wiley.com/en-us/Fundamentals+of+Heat+and+Mass+Transfer%2C+8th+Edition-p-9781119353881.

Birtwell, S., Morgan, H., 2009. Microparticle encoding technologies for high-throughput multiplexed suspension assays. Integrative Biology 1, 345–362. URL: https://doi.org/10.1039/b905502a, doi:10.1039/b905502a.

Buckingham, E., 1914. On Physically Similar Systems; Illustrations of the Use of Dimensional Equations. Physical Review 4, 345–376. URL: https://link.aps.org/doi/10.1103/PhysRev.4.345, doi:10.1103/PhysRev.4.345. publisher: American Physical Society.

Cabrejos, F.J., Klinzing, G.E., 1992. Incipient motion of solid particles in horizontal pneumatic conveying. Powder Technology 72, 51–61. URL: https://www.sciencedirect.com/science/article/pii/S003259109285021M, doi:10.1016/S0032-5910(92)85021-M.

Cabrejos, F.J., Klinzing, G.E., 1994. Pickup and saltation mechanisms of solid particles in horizontal pneumatic transport. Powder Technology 79, 173–186. URL: https://www.sciencedirect.com/science/article/pii/003259109402815X, doi:10.1016/0032-5910(94)02815-X.

Cherukat, P., Mclaughlin, J.B., 1994. The inertial lift on a rigid sphere in a linear shear flow field near a flat wall. Journal of Fluid Mechanics 263, 1–18. URL: https://www.cambridge.org/core/journals/journal-of-fluid-mechanics/article/inertial-lift-on-a-rigid-sphere-in-a-linear-shear-flow-field-near-a-flat-wall/EFAE1B39426002EF83774AF36EC26640, doi:10.1017/S0022112094004015.

Cunin, F., Schmedake, T.A., Link, J.R., Li, Y.Y., Koh, J., Bhatia, S.N., Sailor, M.J., 2002. Biomolecular screening with encoded porous-silicon photonic crystals. Nature Materials 1, 39–41. URL: https://www.nature.com/articles/nmat702, doi:10.1038/nmat702. publisher: Nature Publishing Group.

Eun Chung, S., Ah Lee, S., Kim, J., Kwon, S., 2009. Optofluidic encapsulation and manipulation of silicon microchips using image processing based optofluidic maskless lithography and railed microfluidics. Lab on a Chip 9, 2845–2850. URL: https://pubs.rsc.org/en/content/articlelanding/2009/lc/b903760h, doi:10.1039/B903760H. publisher: Royal Society of Chemistry.

Gibbings, J.C., 2011. Dimensional Analysis. Springer Science & Business Media. URL: https://doi.org/10.1007/978-1-84996-317-6.

Gruda, M.C., Pinto, A., Craelius, A., Davidowitz, H., Kopacka, W.M., Li, J., Qian, J., Rodriguez, E., Kuspiel, E., Mandecki, W., 2010. A system for implanting laboratory mice with light-activated microtransponders. Journal of the American Association for Laboratory Animal Science 49, 826–831. URL: https://www.ingentaconnect.com/content/aalas/jaalas/2010/00000049/00000006/art00007. iSBN: 1559-6109 Publisher: American Association for Laboratory Animal Science.

Halow, J.S., 1973. Incipient rolling, sliding and suspension of particles in horizontal and inclined turbulent flow. Chemical Engineering Science 28, 1–12. URL: https://www.sciencedirect.com/science/article/pii/0009250973850808, doi:10.1016/0009-2509(73)85080-8.

Han, Q., Hunt, J.D., 1995. Particle pushing: critical flow rate required to put particles into motion. Journal of Crystal Growth 152, 221–227. URL: https://www.sciencedirect.com/science/article/pii/0022024895000852, doi:10.1016/0022-0248(95)00085-2.

Hoffmann, D., Brennan, D., Loughran, M., 2006. Injection and manipulation of silicon microbeads in a customized microfluidic platform, in: Microfluidics, BioMEMS, and Medical Microsystems IV, SPIE. pp. 103–110. URL: https://www.spiedigitallibrary.org/conference-proceedings-of-spie/6112/61120E/Injection-and-manipulation-of-silicon-microbeads-in-a-customized-microfluidic/10.1117/12.660342.full, doi:10.1117/12.660342.

Hoffmann, D., Curtin, M., Loughran, M., 2007a. An integrated microsystem for multiplex processing of encoded silicon microbeads, in: Microfluidics, BioMEMS, and Medical Microsystems V, SPIE. pp. 109–116. URL: https://www.spiedigitallibrary.org/conference-proceedings-of-spie/6465/64650D/An-integrated-microsystem-for-multiplex-processing-of-encoded-silicon-microbeads/10.1117/12.702565.full, doi:10.1117/12.702565.

Hoffmann, D., O'Brien, J., Brennan, D., Loughran, M., 2007b. Optically encoded silicon microbeads: Detection and characterisation in a microfluidic system. Sensors and Actuators B: Chemical 122, 653–658. URL: https://www.sciencedirect.com/science/article/pii/S0925400506005016, doi:10.1016/j.snb.2006.07.023.

Hubbe, M.A., 1984. Theory of detachment of colloidal particles from flat surfaces exposed to flow. Colloids and Surfaces 12, 151–178. URL: https://www.sciencedirect.com/science/article/pii/0166662284800967, doi:10.1016/0166-6622(84)80096-7.

Hubert, M., Kalman, H., 2004. Measurements and comparison of saltation and pickup velocities in wind tunnel. Granular Matter 6, 159–165. URL: https://doi.org/10.1007/s10035-004-0166-x, doi:10.1007/s10035-004-0166-x.

Hur, S.C., Choi, S.E., Kwon, S., Carlo, D.D., 2011. Inertial focusing of non-spherical microparticles. Applied Physics Letters 99, 044101. URL: https://doi.org/10.1063/1.3608115, doi:10.1063/1.3608115.

Jensen-McMullin, C., Bachman, M., Li, G.P., 2008. Microfabricated micropallets for enhancement of biomolecular techniques. Microfluidics and Nanofluidics 5, 225–234. URL: https://doi.org/10.1007/s10404-007-0240-x, doi:10.1007/s10404-007-0240-x.

Kalman, H., 2022. Role of Reynolds and Archimedes numbers in particle-fluid flows. Reviews in Chemical Engineering 38, 149–165. URL: https://www.degruyter.com/document/doi/10.1515/revce-2020-0005/html, doi:10.1515/revce-2020-0005. publisher: De Gruyter.

Kalman, H., Satran, A., Meir, D., Rabinovich, E., 2005. Pickup (critical) velocity of particles. Powder Technology 160, 103–

113. URL: https://www.sciencedirect.com/science/article/pii/S0032591005003694, doi:10.1016/j.powtec.2005.08.009.

Karam, M., Saad, T., 2021. BuckinghamPy: A Python software for dimensional analysis. SoftwareX 16, 100851. URL: https://www.sciencedirect.com/science/article/pii/S2352711021001291, doi:10.1016/j.softx.2021.100851.

Krishnan, G.P., Leighton Jr, D.T., 1995. Inertial lift on a moving sphere in contact with a plane wall in a shear flow. Physics of Fluids 7, 2538–2545. URL: https://pubs.aip.org/aip/pof/article-abstract/7/11/2538/457371/Inertial-lift-on-a-moving-sphere-in-contact-with-a, doi:10.1063/1.868755.

Lee, H., Balachandar, S., 2017. Effects of wall roughness on drag and lift forces of a particle at finite Reynolds number. International Journal of Multiphase Flow 88, 116–132. URL: https://www.sciencedirect.com/science/article/pii/S0301932216300994, doi:10.1016/j.ijmultiphaseflow.2016.09.006.

Leighton, D., Acrivos, A., 1985. The lift on a small sphere touching a plane in the presence of a simple shear flow. Zeitschrift für angewandte Mathematik und Physik ZAMP 36, 174–178. URL: https://doi.org/10.1007/BF00949042, doi:10.1007/BF00949042.

Levenberg, K., 1944. A method for the solution of certain non-linear problems in least squares. Quarterly of Applied Mathematics 2, 164–168. URL: https://www.ams.org/qam/1944-02-02/S0033-569X-1944-10666-0/, doi:10.1090/qam/10666.

Li, J., Veltri, R.W., Yuan, Z., Christudass, C.S., Mandecki, W., 2015. Macrophage Inhibitory Cytokine 1 Biomarker Serum Immunoassay in Combination with PSA Is a More Specific Diagnostic Tool for Detection of Prostate Cancer. PLOS ONE 10, e0122249. URL: https://journals.plos.org/plosone/article?id=10.1371/journal.pone.0122249, doi:10.1371/journal.pone.0122249. publisher: Public Library of Science.

Li, J., Wang, Z., Gryczynski, I., Mandecki, W., 2010. Silver nanoparticle-enhanced fluorescence in microtransponder-based immuno- and DNAhybridization assays. Analytical and Bioanalytical Chemistry 398, 1993–2001. URL: https://doi.org/10.1007/s00216-010-4108-7, doi:10.1007/s00216-010-4108-7.

Liga, A., Morton, J.A.S., Kersaudy-Kerhoas, M., 2016. Safe and cost-effective rapid-prototyping of multilayer PMMA microfluidic devices. Microfluidics and Nanofluidics 20, 164. URL: https://doi.org/10.1007/s10404-016-1823-1, doi:10.1007/s10404-016-1823-1.

Lin, X., Flint, J.A., Azaro, M., Coradetti, T., Kopacka, W.M., Streck, D.L., Wang, Z., Dermody, J., Mandecki, W., 2007. Microtransponder-Based Multiplex Assay for Genotyping Cystic Fibrosis. Clinical Chemistry 53, 1372–1376. URL: https://doi.org/10.1373/clinchem.2006.081810, doi:10.1373/clinchem.2006.081810.

Mandecki, W., Ardelt, B., Coradetti, T., Davidowitz, H., A. Flint, J., Huang, Z., M. Kopacka, W., Lin, X., Wang, Z., Darzynkiewicz, Z., 2006. Microtransponders, the miniature RFID electronic chips, as platforms for cell growth in cytotoxicity assays. Cytometry Part A 69A, 1097–1105. URL: https://onlinelibrary.wiley.com/doi/abs/10.1002/cyto.a.20344, doi:10.1002/cyto.a.20344.

Marquardt, D.W., 1963. An Algorithm for Least-Squares Estimation of Nonlinear Parameters. Journal of the Society for Industrial and Applied Mathematics 11, 431–441. URL: https://epubs.siam.org/doi/10.1137/0111030, doi:10.1137/0111030. publisher: Society for Industrial and Applied Mathematics.

Martinez, R.C., Sweeney, L.G., Finlay, W.H., 2009. Aerodynamic Forces and Moment on a Sphere or Cylinder Attached to a Wall in a Blasius Boundary Layer. Engineering Applications of Computational Fluid Mechanics 3, 289–295. URL: https://doi.org/10.1080/19942060.2009.11015272, doi:10.1080/19942060.2009.11015272. publisher: Taylor & Francis _eprint: https://doi.org/10.1080/19942060.2009.11015272.

Palakurthi, N.K., Ghia, U., Turkevich, L., 2017. Simulations of Particle Detachment From a Flat Surface, American Society of Mechanical Engineers Digital Collection. URL: https://dx.doi.org/10.1115/FEDSM2017-69111, doi:10.1115/FEDSM2017-69111.

Patankar, N.A., Huang, P.Y., Ko, T., Joseph, D.D., 2001. Lift-off of a single particle in Newtonian and viscoelastic fluids by direct numerical simulation. Journal of Fluid Mechanics 438, 67–100. URL: https://www.cambridge.org/core/journals/journal-of-fluid-mechanics/article/abs/liftoff-of-a-single-particle-in-newtonian-and-viscoelastic-fluids-by-direct-numerical-simulation/63BD4F6A162DBB192DA0A1C0E7B0B5A5, doi:10.1017/S0022112001004104.

Rabinovich, E., Kalman, H., 2007. Pickup, critical and wind threshold velocities of particles. Powder Technology 176, 9–17. URL: https://www.sciencedirect.com/science/article/pii/S0032591007000496, doi:10.1016/j.powtec.2007.01.033.

Rabinovich, E., Kalman, H., 2008. Generalized master curve for threshold superficial velocities in particle–fluid systems. Powder Technology 183, 304–313. URL: https://www.sciencedirect.com/science/article/pii/S0032591007003798, doi:10.1016/j.powtec.2007.07.030.

Rabinovich, E., Kalman, H., 2009a. Incipient motion of individual particles in horizontal particle–fluid systems: A. Experimental analysis. Powder Technology 192, 318–325. URL: https://www.sciencedirect.com/science/article/pii/S0032591009000618, doi:10.1016/j.powtec.2009.01.013.

Rabinovich, E., Kalman, H., 2009b. Incipient motion of individual particles in horizontal particle–fluid systems: B. Theoretical analysis. Powder Technology 192, 326–338. URL: https://www.sciencedirect.com/science/article/pii/S003259100900062X, doi:10.1016/j.powtec.2009.01.014.

Rich, R., Li, J., Fudala, R., Gryczynski, Z., Gryczynski, I., Mandecki, W., 2012. Properties of coatings on RFID p-Chips that support plasmonic fluorescence enhancement in bioassays. Analytical and Bioanalytical Chemistry 404, 2223–2231. URL: https://doi.org/10.1007/s00216-012-6369-9, doi:10.1007/s00216-012-6369-9.

Shukla, N., Henthorn, K.H., 2009. Effect of relative particle size on large particle detachment from a microchannel. Microfluidics and Nanofluidics 6, 521–527. URL: https://doi.org/10.1007/s10404-008-0330-4, doi:10.1007/s10404-008-0330-4.

Slocum, A., 2010. Kinematic couplings: A review of design principles and applications. International Journal of Machine Tools and Manufacture 50, 310–327. URL: https://www.sciencedirect.com/science/article/pii/S0890695509002090, doi:10.1016/j.ijmachtools.2009.10.006.

Stevenson, P., Thorpe, R.B., Davidson, J.F., 2002. Incipient motion of a small particle in the viscous boundary layer at a pipe wall. Chemical Engineering Science 57, 4505–4520. URL: https://www.sciencedirect.com/science/article/pii/S0009250902004189, doi:10.1016/S0009-2509(02)00418-9.

Stojimirović, B., Galli, M., Trefalt, G., 2020. Forces between silica particles in isopropanol solutions of 1:1 electrolytes. Physical Review Research 2, 023315. URL: https://link.aps.org/doi/10.1103/PhysRevResearch.2.023315, doi:10.1103/PhysRevResearch.2.023315. publisher: American Physical Society.

Truskey, G.A., Yuan, F., Katz, D.F., 2004. Transport phenomena in biological systems. URL: https://www.pearson.com/en-us/subject-catalog/p/transport-phenomena-in-biological-systems/P200000003212/9780131569881. publisher: Pearson/Prentice Hall Upper Saddle River, NJ, USA:.

Vastl, J., Wang, T., Trinh, T.B., Spiegel, D.A., 2017. Encoded Silicon-Chip-Based Platform for Combinatorial Synthesis and Screening. ACS Combinatorial Science 19, 255–261. URL: https://doi.org/10.1021/acscombsci.6b00181, doi:10.1021/acscombsci.6b00181. publisher: American Chemical Society.

Xiao, X.Y., Li, R., Zhuang, H., Ewing, B., Karunaratne, K., Lillig, J., Brown, R., Nicolaou, K., 2000. Solid-phase combinatorial synthesis using MicroKan reactors, Rf tagging, and directed sorting. Biotechnology and Bioengineering 71, 44–50. URL: https://onlinelibrary.wiley.com/doi/abs/10.1002/%28SICI%291097-0290%28200024%2971%3A1%3C44%3A%3AAID-BIT7%3E3.0.CO%3B2-J, doi:10.1002/(SICI)1097-0290(200024)71:1<44::AID-BIT7>3.0.CO;2-J.

Zeng, L., Najjar, F., Balachandar, S., Fischer, P., 2009. Forces on a finite-sized particle located close to a wall in a linear shear flow. Physics of Fluids 21. URL: https://pubs.aip.org/aip/pof/article-abstract/21/3/033302/257046/Forces-on-a-finite-sized-particle-located-close-to?redirectedFrom=fulltext, doi:10.1063/1.3082232.

Supplementary Material for: Characterization of the critical lift-off of a single flat-plate microchip particle in straight rectangular microchannel flows

Raymond Yeung[a], Cynthia Sainz[b], Jason Mandala[c],
Philip Brisk[d], William H. Grover[a], Victor G. J. Rodgers[a,*]

[a]*Department of Bioengineering, University of California, Riverside, Riverside, 92521, CA, USA*
[b]*Department of Evolution, Ecology, and Organismal Biology, University of California, Riverside, Riverside, 92521, CA, USA*
[c]*Department of Electrical and Computer Engineering, University of California, Riverside, Riverside, 92521, CA, USA*
[d]*Department of Computer Science and Engineering, University of California, Riverside, Riverside, 92521, CA, USA*

S1. Friction coefficient of particle surfaces

The single-sided patterning of silicon wafers for fabrication of p-Chip microtransponders leads to a non-uniformity of the p-Chip surfaces. The active side of the p-Chip is patterned with layers forming integrated circuits and the substrate side has no patterning. Orientation of the p-Chip surface relative to bottom channel wall cannot be consistently controlled during particulate flow experiments. Therefore, the friction coefficient between the particle surface and the wall needs to be evaluated for both major surfaces of the particle to ensure the surface orientation of the p-Chip does not significantly affect the observed particle lift-off. Inclined plane tests were performed to evaluate the particle-wall friction coefficients using a direct measuring approach (Coetzee, 2016, 2020) involving placement of a single p-Chip immersed with deionized water, positioned along the middle of the channel length to eliminate entrance/end effects and near the axial centerline to minimize wall effects, on the bottom surface of an angled, rectangular, poly(methyl methacrylate) (PMMA) microchannel. The static friction coefficient, μ_{sf}, may be determined from the angle at which the particle begins to move from rest. The kinetic friction coefficient, μ_{kf}, may be evaluated from the angle at which the particle moves at constant velocity. Tests were repeated five times for each of the two major surface orientations. Angles were analyzed using MATLAB 2023a (MathWorks, Natick, MA, USA). In the experimental tests, the static friction coefficients between the particle and wall could not be evaluated due to the significant adhesion from electrostatic forces. However, the values for μ_{kf} between the particle and wall were determined following initiation of movement from rocking agitation. The values for μ_{kf} were 0.222 ± 0.007 and 0.216 ± 0.008 for particle-wall contact with the active and substrate surfaces, respectively. Therefore, the difference between μ_{kf} with respect to the two major particle surfaces was determined to be insignificant and the particle was treated as uniform for our analysis. Based on previous studies of non-spherical sand corresponding to the same size as the p-Chip, we assumed the value of μ_{sf} between the particle and wall as 0.7 (Rabinovich and Kalman, 2009).

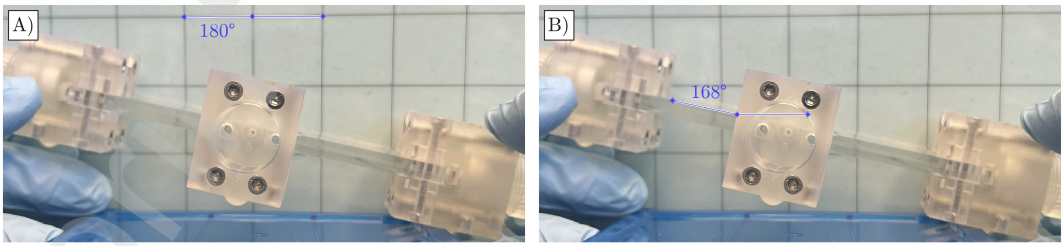

Figure S1: Experimental direct measuring of friction coefficients between the major particle surface and the bottom channel wall. After initiation of particle motion with agitation, the device was angled such that the particle moves at a constant velocity. A) Calibration of the horizontal reference line. B) Measurement of the device angle to evaluate the kinetic friction coefficient between the contacting particle surface and the channel wall.

*Corresponding author
Email address: victor.rodgers@ucr.edu (Victor G. J. Rodgers)

References

Coetzee, C., 2020. Calibration of the discrete element method: Strategies for spherical and non-spherical particles. Powder Technology 364, 851–878. URL: https://www.sciencedirect.com/science/article/pii/S0032591020300899, doi:10.1016/j.powtec.2020.01.076.

Coetzee, C.J., 2016. Calibration of the discrete element method and the effect of particle shape. Powder Technology 297, 50–70. URL: https://www.sciencedirect.com/science/article/pii/S0032591016301620, doi:10.1016/j.powtec.2016.04.003.

Rabinovich, E., Kalman, H., 2009. Incipient motion of individual particles in horizontal particle–fluid systems: A. Experimental analysis. Powder Technology 192, 318–325. URL: https://www.sciencedirect.com/science/article/pii/S0032591009000618, doi:10.1016/j.powtec.2009.01.013.